2017

Development of a novel, bicombinatorial approach to alloy development, and application to rapid screening of creep resistant titanium alloys

Brian William Martin
Iowa State University

Development of a novel, bicombinatorial approach to alloy development, and application to rapid screening of creep resistant titanium alloys

by

Brian Martin

A thesis submitted to the graduate faculty

in partial fulfillment of the requirements for the degree of

MASTER OF SCIENCE

Major: Materials Science and Engineering

Program of Study Committee:
Peter Collins, Major Professor
Iver Anderson
Frank Peters

The student author, whose presentation of the scholarship herein was approved by the program of study committee, is solely responsible for the content of this thesis. The Graduate College will ensure this thesis is globally accessible and will not permit alterations after a degree is conferred.

Iowa State University
Ames, Iowa
2017

DEDICATION

To Evelyn.

You have done more for me than you know, and this would have been impossible without your love and support.

TABLE OF CONTENTS

LIST OF FIGURES

LIST OF TABLES

ACKNOWLEDGEMENTS

Firstly, I need to thank my adviser, Dr. Peter Collins, without whom this work would be impossible. He had taken the chance on my joining his group, and continued to provide invaluable support throughout my work. I aspire to be half the scientist he is, and to someday call him a peer.

The fellow members of Dr. Collins's group have been a great resource for knowledge and friendship throughout my tenure. David Brice and Thomas Ales, who convinced Dr. Collins to hire me in the first place, for their extensive knowledge of metallurgy, electron microscopy and additive manufacturing, and continued assistance up to editing this document. Dr. Peyman Samimi, whose work was the starting point for much of this work, and continued to lend his expertise on the LENS and other areas to my efforts. Michael Mendoza, Matthew Kenney, Muchen Li, Alden Watts, and Dr. Iman Ghamarian have all been sources for intelligent insight and friendship.

My funding source, the Center for Advanced, Non-Ferrous, Structural Alloys (CANFSA), but more importantly, the industrial mentors who used their experience and expertise to shaping this project. My project mentor, Dr. John Foltz, was especially helpful in lending his expertise in titanium metallurgy and enthusiasm for research.

I'd like to thank the U.S. DOE Ames Laboratory for supporting this work, in part, by contributing to the fabrication of samples through the use of the LENS, and the housing of the Gleeble, through its Materials Preparation Center.

Finally, my parents and family. Their guidance has made me the person I am today, and I hope I have made them proud.

ABSTRACT

Combinatorial approaches have proven useful for rapid alloy fabrication and optimization. A new method of producing controlled isothermal gradients using the Gleeble Thermomechanical simulator has been developed, and demonstrated on the metastable β-Ti alloy β-21S, achieving a thermal gradient of 525-700° C. This thermal gradient method has subsequently been coupled with existing combinatorial methods of producing composition gradients using the LENS^{TM} additive manufacturing system, through the use of elemental blended powders. This has been demonstrated with a binary Ti-(0-15) wt% Cr build, which has subsequently been characterized with optical and electron microscopy, with special attention to the precipitate of $TiCr_2$ Laves phases. The $TiCr_2$ phase has been explored for its high temperature mechanical properties in a new oxidation resistant β-Ti alloy, which serves as a demonstration of the new bicombinatorial methods developed as applied to a multicomponent alloy system.

CHAPTER 1. INTRODUCTION

While metal 3D printing, or Additive Manufacturing (AM), has existed in prototype and laboratory scale systems since the 1980s, it is really only in the past several years that it has come into its own as a viable tool in manufacturing and prototyping. The short lead time on new part geometries, flexibility of part geometry, and minimal waste of materials are all factors that have led to its increased use in manufacturing and machining. While metallurgical study and certification of the processes themselves is an entirely new field on its own, the nature of the rapid fabrication means that additive manufacturing systems are a valuable new tool for materials scientists and engineers. Methods have been developed where composition gradients are used to study microstructure, properties, and behavior changes in a single, rapidly fabricated sample.

The production of a large number of samples across a wide range of process and property variation is often referred to as a "combinatorial approach", usually applied to changes in composition. Here, this concept of combinatorial materials science is extended to include the design and application for graded, isothermal holds on metal specimens, and the subsequent study of the effects on microstructure and properties that result from such thermal gradients. This has been developed and validated using a metastable β Ti alloy, β-21S, achieving a temperature range of ~175° C. This is then coupled with the composition gradient methods, in the form of a Ti-Cr binary alloy gradient with perpendicular thermal gradient of ~125° C, to produce a new, bicombinatorial technique for rapid alloy characterization, and development.

These techniques developed were subsequently applied to real world problems, in the form of high temperature performance of β-Ti alloys. β-21S, an alloy developed specifically for high temperature oxidation resistance, was selected as a baseline alloy to improve the creep

properties of these β alloys. These β alloys typically exhibit poorer oxidation resistance and mechanical performance at high temperatures when compared to α and α/β alloys, and the $TiCr_2$ Laves phase was explored for their potential to improve the mechanical properties of the oxidation resistant alloys.

The Gleeble Thermomechanical simulator was used for both the application of controlled thermal gradients, as well as the creep testing. The resistive heating capabilities, when applied to controlled geometry, allowed for the careful application of the linear thermal gradients. The thermomechanical capabilities were also exploited for rapid creep performance screening, using Larson-Miller parameters to provide a first evaluation of the new alloys. While the creep performance of the $TiCr_2$ based as-cast alloys was poorer than the β-21S, these studies could still lead to a new class of alloys.

CHAPTER 2. LITERATURE REVIEW

This thesis covers the development of new tools for combinatorial materials science alloy development, specifically to new titanium systems. The literature review will then cover three main sections. Firstly, an overview of titanium metallurgy is given, with a focus on the β class, as well as deeper discussion on the Ti-Cr eutectic system. Secondly, a discussion of creep in β titanium alloys, which serve as a motivation factor for the development of new combinatorial methods. Lastly, an overview of the development of the LENS^{TM} additive manufacturing system as a tool for combinatorial alloy development is given, followed by some previous applications of the LENS^{TM} in furthering the understanding of titanium metallurgy.

Titanium Metallurgy

Alloy classification

Pure titanium forms two distinct thermodynamically stable phases, with the transition occurring at 882° C. The low temperature α phase is a hexagonal close packed (hcp) structure with lattice parameters a = 0.295 nm and c = 0.468 nm. The high temperature β phase is body centered cubic (bcc) with a lattice parameter of 0.332 nm. The addition of various alloying elements can stabilize either phase, resulting in either a lowering or raising of the β transition temperature. Some common α stabilizers include Al and O, and common β stabilizers include V, Nb, Ta, Cr, Mo, W, Mn, Fe, Co and Ni [1]. Neutral stabilizers, which have little to no effect on the transition temperature with increasing concentration, include Sn and Zr. Different alloys of titanium are classified according to the relative abundance of either α or β stabilizing elements, and the subsequent fraction of the α or β phases present.

While the effects of alloying elements in multicomponent titanium alloy systems have numerous interrelated aspects, and in reality the various elemental components interact to do

more than simply stabilize one phase or the other irrespective of tertiary or quaternary alloying additions, it is nonetheless useful to implement an effective abundance of some well-known α or β stabilizer to represent the effect of all the alloying elements. This was first developed by Rosenberg for α stabilizers [2], where an equivalent Al abundance, termed the Al equivalency, can be calculated (Equation 1). Collings used data from Molchanova [3] to develop an similar equation for β stabilizers, using a Mo equivalency (Equation 2) [4].

$$[Al]_{eq} = [Al] + 0.17[Zr] + 0.33[Sn] + 10[O] \quad \text{Eq. 1}$$

$$[Mo]_{eq} = [Mo] + 0.2[Ta] + 0.28[Nb] + 0.4[W] + 0.67[V] + 1.25[Cr] + 1.25[Ni] + 1.7[Mn] + 1.7[Co] + 2.5[Fe] \quad \text{Eq. 2}$$

Used together, these equations are a good qualitative tool to have when studying alloy systems in titanium.

Figure 0.1 shows a prototypical schematic phase diagram, dividing the alloy classification by the room temperature stability of the two phases with respect to concentration, as well as the martensitic transition temperature. Titanium alloys that are almost entirely hcp α, and contain primarily α stabilizers, are referred to as α alloys. These include commercially pure (CP) titanium, with varying allowable impurities of Fe or O, and Ti-5Al-2.5Sn. While these alloys frequently exhibit satisfactory mechanical properties such as strength, toughness, and weldability, they are primarily useful for the superior corrosion resistance of α titanium, especially at elevated temperatures [1,4,5].

Alloys with both stable α and β phases that retain the martensitic phases upon quenching to room temperature are known as α/β alloys. These alloys support a mixed microstructure of both α and β phases, resulting in increased strength compared to α alloys [5]. The most commonly used titanium alloy, Ti-6Al-4V, or Grade 5, is an α/β alloy. This class also has

excellent toughness and corrosion resistance, along with good formability and weldability. In addition, unlike α alloys, these alloys can be heat treated and aged to increase strength, meaning the final mechanical properties can be adjusted according to specific applications.

Metastable β alloys contain enough alloying element additions that the β phase is retained on quenching from the β phase field. This β is then metastable, and will precipitate α with appropriate thermal treatments. These treatments allow for a large amount of careful tailoring of the microstructure and properties to be done after the alloy has been worked [1,5]. These alloys can also be cold rolled, strip rolled, and forged at lower temperatures, making them easier to work and manufacture compared to α or α/β alloys.

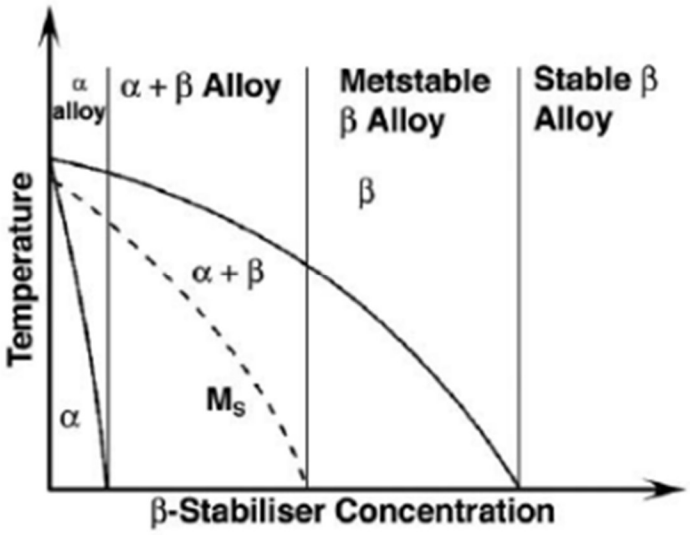

Figure 0.1- Schematic isomorphous phase diagram showing titanium alloy classification [1]

Titanium-chromium system

Overall, the phase stability in the Ti-rich side of the system is well studied, as reviewed by Murray [6] and Cupid et al. [7]. Figure 0.2 shows the equilibrium phase diagram of the system given by Cupid, et al. showing the eutectoid at 686° C and 12 wt% Cr [7]. When

quenched from the β phase field, Ti-rich portions form martensite of α. Unlike many other β stabilized Ti systems, the orthorhombic α'' is not found in Ti-Cr, and only the hexagonal α' is formed [8]. Above certain concentrations of Cr, there is enough to fully stabilize the β phase in the quenched condition (Figure 0.1). Murray [6] reports several studies, which show a range of 9.3-3.7 at%, while Williams [1] states approximately 7.4 at% is sufficient. All reported values are below the eutectoid composition of 12 wt% Cr.

As a eutectoid β stabilizer of Ti, in addition to α and β phases being stable, there is the presence of intermetallic ordered structure in the form of the three Laves phases, shown in: low temperature cubic $MgCu_2$ (C15, marked as $TiCr_2$ rt in Figure 0.2), high temperature hexagonal $MgZn_2$ (C14, marked as $TiCr_2$ ht2), and intermediate temperature hexagonal $MgNi_2$ (C36, marked as $TiCr_2$ ht1). The presence of all three Laves phase variants in a single binary system is unusual, with the C36 intermediate variant not recognized in earlier work done on the system [6]. These phases are stable, and once formed do not easily transform. Murray also states that "these structures can be described as different stacking sequences of the same basic cell, and small amounts of one phase may easily be interpreted as stacking fault variants of another" [6]. For this reason, the Laves phase compound region is still largely regarded as speculative [6,7]. Also leading to difficulty regarding the behavior of the formation of these Laves phases is that they do not form immediately upon ageing in the α+$TiCr_2$ phase field. They have been observed to have relatively sluggish kinetics, and require prolonged ageing for the α and β to form them [9–11], with one proposed sequence of α' -> α + β -> α + β + $TiCr_2$ [12].

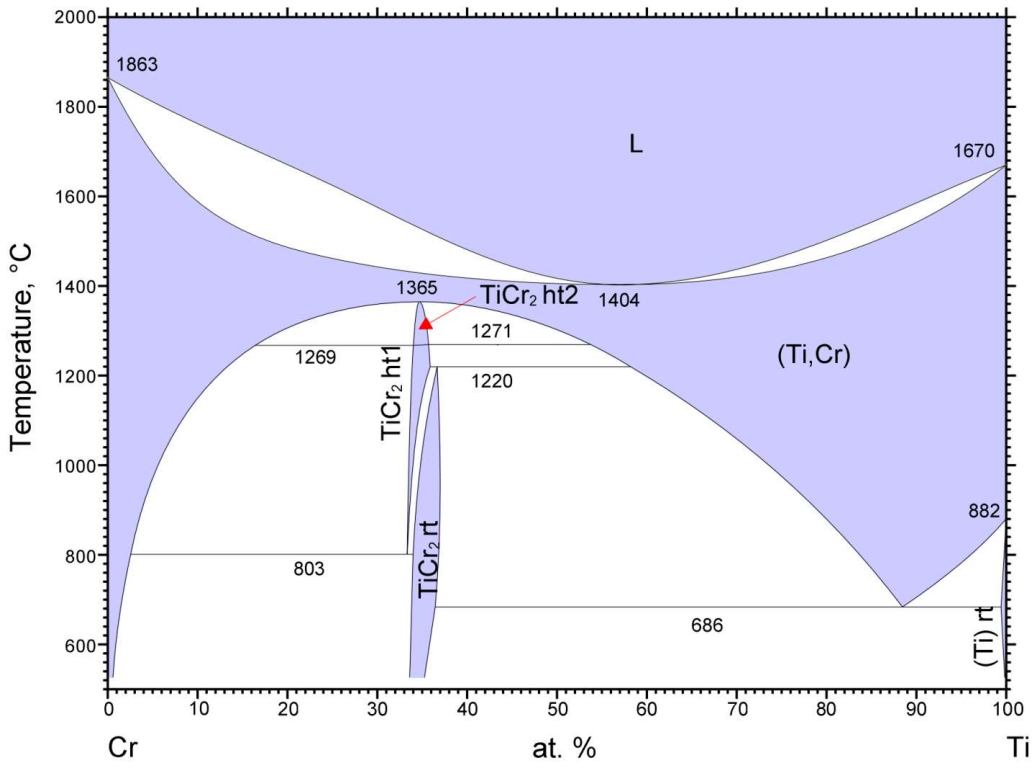

Figure 0.2 – Equilibrium phase diagram of Ti-Cr system [7]. Taken from ASM Alloy Phase Diagram Database.

Despite problems of brittleness at room temperature, the $TiCr_2$ phase, and Laves phases in general, have shown to exhibit promising high temperature mechanical properties [9,10] Chen, et al. studied hardness and fracture toughness in the Ti-Cr alloy space, including exploring effects of ternary additions and two-phase binary alloys containing $TiCr_2$ [10]. One aspect of the $TiCr_2$ laves formation that bears special mention is that, unlike many other of the Laves phases, which precipitate from a liquid in a eutectic or peritectic decomposition, the Ti-Cr system forms from solid solution bcc via a eutectoid. The $TiCr_2$ phases are also attractive for having a solubility range, where 75% of other Laves phases exist as line compounds [13]. This allows more flexibility in the microstructural control, and if favorable properties of this system are found, they would be more industrially relevant. Chen found that formation of the Laves phase in

conjunction with a Ti-Cr bcc improved the toughness, where crack length in the Laves particles was limited by the bcc phase. Chen also found the addition of ternary elements that dissolve in both bcc and Laves phase, such as Mo, V, Nb and Fe, improve toughness. The addition of ternary elements is supported by additional studies, which showed ternary elements that served as substitutional solutes improved ductility though disruption and relaxation of the close-packed structure [10,14].

Creep in β Titanium Alloys

Creep is defined as time-dependent plasticity, where at elevated temperatures and constant stress, materials exhibit a non-zero strain rate. Typically, this occurs at temperatures greater than $0.5T_m$, with T_m being the absolute melting temperature [15]. Figure 0.3 shows a schematic of a classical strain – time curve for creep. The three regions are often termed primary (Stage I), secondary (Stage II), and tertiary (Stage III) creep. Stage I creep is marked by a decrease in the strain rate with increasing strain, as the material is work hardened and the flow stresses increase [15]. Stage II creep occurs when the hardening is enough to halt changes in the strain rate, and a minimum strain rate, also referred to as steady-state strain rate, is reached. This "minimum creep rate" is often focused on when discussing creep, as secondary stage creep traditionally dominates the creep behavior of structural alloys [16]. Stage III creep occurs when cavitation and cracking once again increase the strain rate, eventually leading to failure.

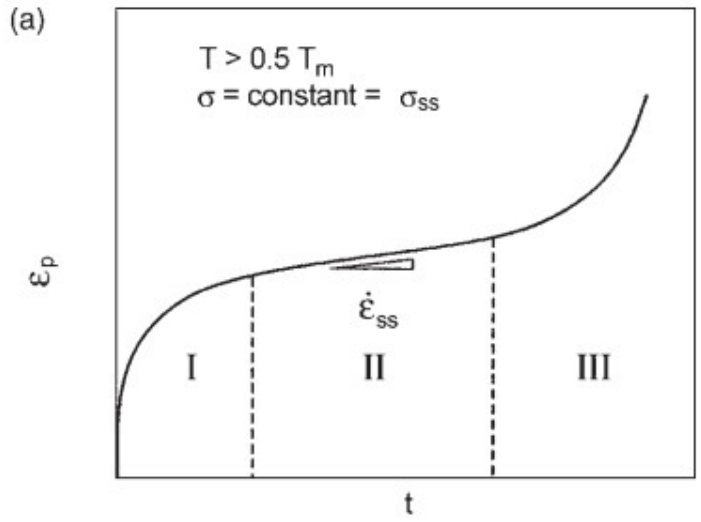

Figure 0.3 – Schematic of a typical strain-time creep curve [15].

Creep mechanisms

A major reason that creep is such a difficult phenomenon to incorporate into design rules and predict is that it is described by several different mechanisms, each itself defined by specific stresses, and temperatures. The main mechanisms are dislocation climb, dislocation glide, Coble creep and Nabarro-Herring creep [16], described below.

Coble and Nabarro-Herring

Coble and Nabarro-Herring creep both deal with the diffusion, due to applied stress, of atoms and vacancies in a crystal lattice (Figure 0.4). At lower stress levels and lower temperature, Coble creep is usually the dominant mechanism. Here, atoms and vacancies diffuse along grain boundaries, due to the higher energy of the atoms at these boundaries, where less activation energy is required to induce diffusional flow. As the temperature is increased, the difference in energy states becomes less important, and diffusion within the bulk of the grain, where more atoms are available to diffuse, dominates. This intragranular diffusion is described by Nabarro-Herring creep [16].

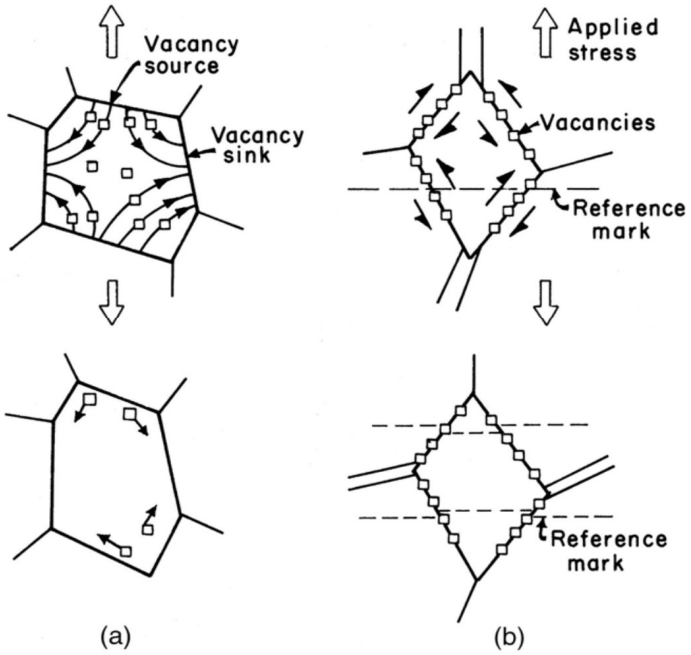

Figure 0.4 – Representation of a) Nabarro-Herring and b) Coble creep [17].

Dislocation creep

The movement of dislocations is the defining feature of plastic flow. At elevated temperatures and higher stress, dislocations can diffuse across glide planes in mechanisms known as dislocation climb. At lower temperatures and higher stress, dislocations will not climb, but can still flow and induce creep deformation.

Creep testing

Testing for creep requires the application of a constant load or stress to a specimen, while it is simultaneously held at a constant elevated temperature. Figure 0.5 shows schematic of a simple constant load creep tester, with a heating element held around the sample. These types of tests often are run to failure.

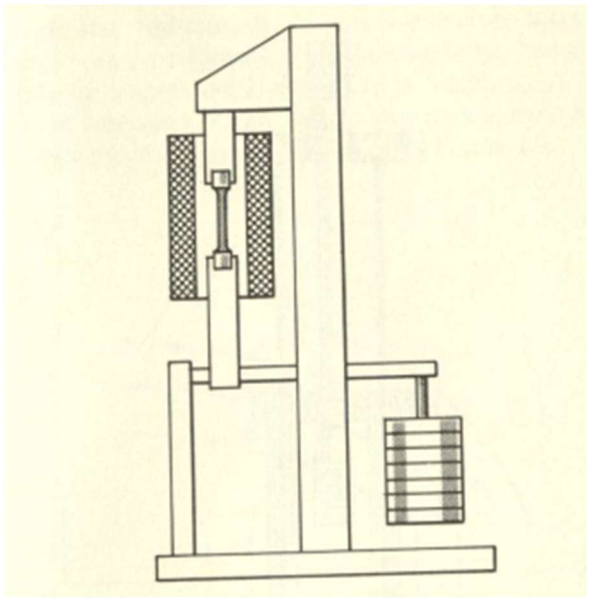

Figure 0.5 – Constant force load frame schematic used for standard creep tests, including a heating element surrounding the specimen [18].

Due to creep being dependent on material properties (e.g. grain size, composition, microstructure, phase stability, melting temperature, yield stress), stress and temperature, there is often difficulty in representing creep data in a meaningful way. A method to compensate for this is the use of the Larson-Miller parameter, which combines temperature and time into a single parameter [19]. Figure 0.7 shows one of these Larson-Miller plots, showing creep performance of several Ti alloys. In this example, the "t" used is time to 0.2% strain, but time to failure is also a commonly used parameter.

Recently, thermomechanical simulators have been used in an attempt to provide a new method of creep testing. These systems use resistive heating to rapidly heat and cool metallic specimens, and provide fine-tuned control of their thermal history. Work done by Peterson [20] used an Electro Thermomechanical Tester (ETMT) to perform creep tests. The ETMT uses resistive heating to heat the sample, and thermocouples welded directly to the surface for rapid heating and closer control of the thermal state of the sample in question. Relevant to increased

use of resistive heaters, Peterson found that an applied current to the sample had a direct and repeatable effect on the creep rate. Using both resistive heating mechanisms as well as traditional inductive heating to keep the temperature constant, Peterson showed that increasing the applied current increased the creep rate by 10-fold (Figure 0.6). Peterson posits this to be an electron wind effect, where the flow of electrons due to the current is contributing to either mass diffusion or dislocation motion. However, Peterson still observed the expected trends when testing various Ti-alloys, and was able to use the ETMT to effectively study the effects of compositional variation on the creep performance of β-Ti alloys (Figure 0.7).

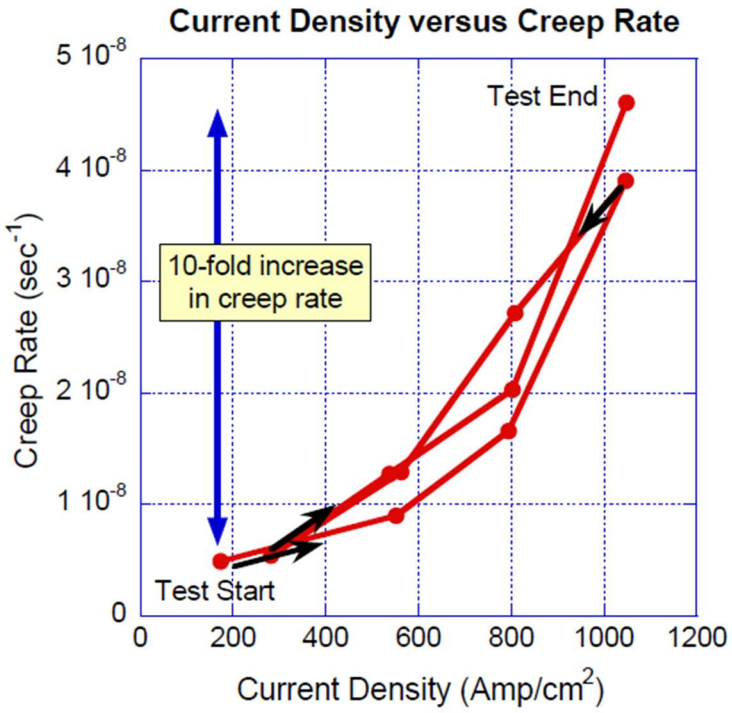

Figure 0.6 – Study of effect of current density on creep rate in ETMT [20].

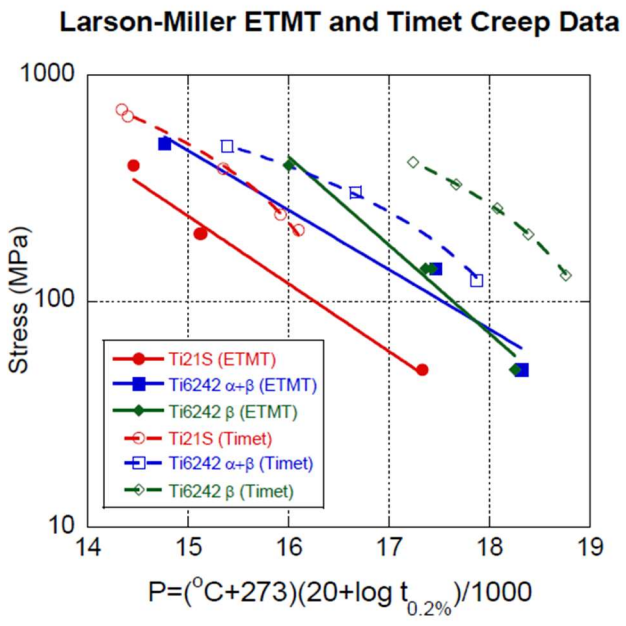

Figure 0.7 – Larson-Miller plot for several Ti alloys, testing in ETMT and using traditional methods [20].

Creep in β Ti

Given that most applications for Ti alloys, and especially β Ti alloys, is at elevated temperature, creep is often a major limiting factor on the use of these alloys. Titanium has also been observed to exhibit creep at lower temperatures than other structural alloys, showing significant strain at $0.4T_m$ [21–23]. β has even worse creep performance than α, usually attributed to the much faster diffusion rates in bcc versus hcp crystal structure [1,24]. The rate controlling mechanisms for creep in titanium is largely dislocation based: glide or climb [4]. In metastable β alloys, the movement of dislocations is largely inhibited by the α/β interfaces, so the morphology of the α phase precipitates is the critical microstructural feature controlling the creep behavior. Work done by Ponsonnet [21] showed the effect of the α phase morphology on the creep behavior of β-CEZ, a near β alloy. This work confirmed the α formation as being the primary rate controlling feature for dislocation motion, where solutionization in the β phase field

followed by a short, low temperature age in the α/β region to form small, finely dispersed α. Ultimately, this served to both increase the volume fraction of α, as well as the surface area of the α/β interfaces.

Other additions and secondary phases can result in increased creep strength. The addition of Si is frequently found in creep resistant β-titanium alloys, such as β-21S [25]. Generally, small amounts have been found to improve creep properties, in both solution and formation of silicides [26]. The presence of other intermetallic compounds, such as the $TiCr_2$ Laves phase precipitated with α in a β matrix has also been shown to improve creep [27]. In both of these cases, the inhibition of dislocation motion is the operable mechanism.

Combinatorial Materials Science using LENS™

The term "combinatorial", when used in the context of materials science, refers to the fabrication of many samples across a range of various parameters (e.g. composition, annealing time or temperature, ageing time or temperature, cold or hot working), in order to parse out previously unseen trends, optimize properties, or otherwise study changes across a wide range of some process variable. The LENS™ (Laser Engineered Net Shaping) system, developed and manufactured by Optomec, is a powder fed, laser melted, additive manufacturing system that expanded the realm of possibilities for combinatorial studies in new and exciting ways. Using multiple powder feeders containing blends of elemental metal powders with varying composition, it is possible to deposit a sample with several compositions in continuous layers. The ability to fabricate a compositionally graded sample has been useful for the study of questions directly relevant to materials science.

Development of the LENS^{TM} as a combinatorial tool

The first work done demonstrating the possibility of using blended elemental powder in a metal AM system was done by Takeda and Steen [28,29] with Fe-Cr-Ni and Fe-Co-Al systems respectively, in the context of developing laser cladding technology. Takeda, et al. [28] investigated using several different powder delivery systems: one hopper with mixed elemental powder, three hoppers of elemental powder that fed into a single delivery pipe, and three hoppers with three delivery pipes. In all cases, the setup of having metal powder blown via inert gas to a melt pool generated by a focused laser onto a build plate was the same. They observed that compositional inhomogeneity resulted from too high of a movement speed, suggesting melt time is an important factor to provide complete mixing. Steen, et al. [29] made use of the three hoppers feeding into a single delivery tube developed by Takeda. They also implemented automatic calibration of the flow rates of the hoppers, as shown in Figure 0.8. Flow rate measurements meant that they could accurately control the final composition before it was deposited, and by adjusting the flow rate of a certain element, deposit a single track with a gradient in composition. This was used to study the effect of varying levels of Co on pitting resistance.

While these studies laid the groundwork for future work in rapid alloy screening using this method, including investigation into the effects of motor speed on powder flow rate and homogeneity issues from incomplete mixing or melting, issues such as the effect of melting temperature, enthalpy of mixing of alloying components, and overall power input per unit area were not considered. These studies were similarly limited in their dimensional capabilities. The directed laser deposition for these studies did not have capabilities to move up or down (Z

direction), merely in an X-Y plane. Thus, they were limited to laser cladded or surface type properties, and could not easily translate to studying bulk microstructure or properties

The commercial availability of the LENS^{TM} system meant that these techniques (variable flow rate to control composition, elemental powder blends and in situ alloying) became more accessible, and useful for more costly alloy systems such as Ti. Shwendner, et al. [30] worked to apply in situ alloying to the LENS^{TM}, and studied effects of the enthalpy of mixing on the homogeneity of the deposited material. A negative enthalpy of mixing results in an exothermic reaction at the melt pool, contributing to the heat of the system and resulting in more reliable mixing and melting of the powder. A positive enthalpy of mixing, on the other hand, resulted in the opposite, where additional energy input is required to melt, and then mix, the constituent powders. Using Ti-10Cr, which has negative enthalpy of mixing, and Ti-10Nb, which has positive enthalpy of mixing, as test cases, Schwendner et al. showed the importance of these thermodynamic considerations seen in Figure 0.9. Here, the Ti-Cr builds were fully homogenized and melted, where the Ti-Nb builds had large numbers of unmelted, unmixed particles.

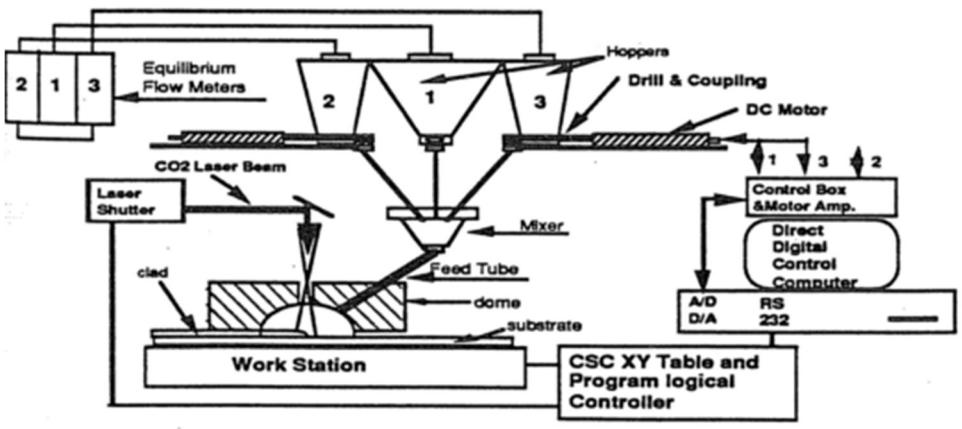

Figure 0.8- Schematic of setup used by Steen, et al. [29]*, showing triple hopper powder feeder with automatically calibrated powder flow rates.*

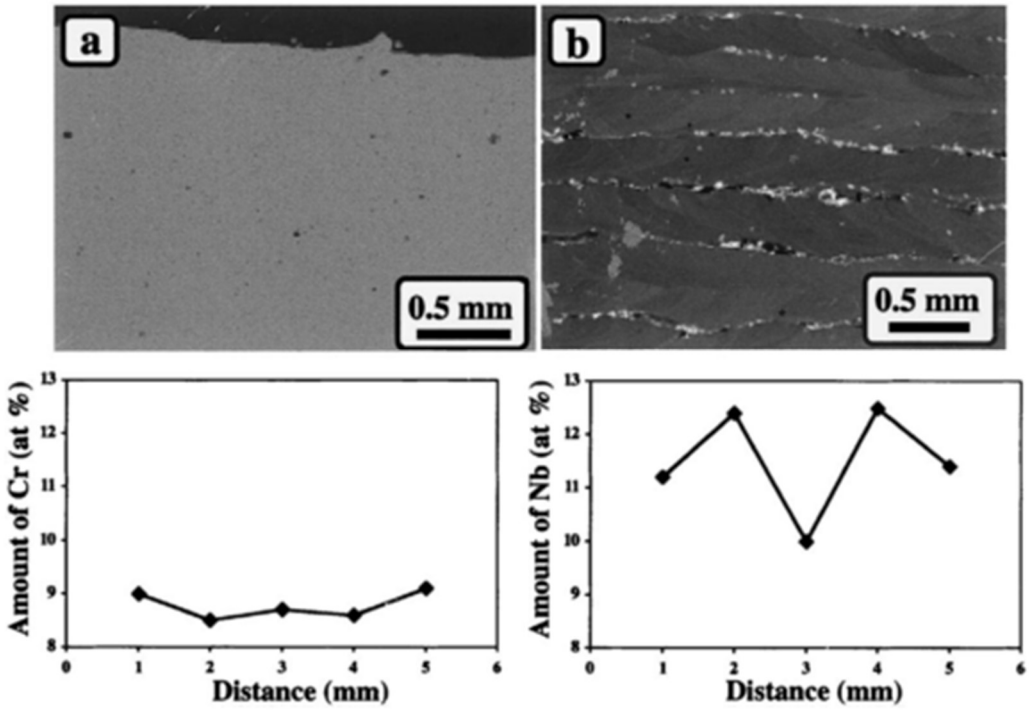

Figure 0.9 – Effect of enthalpy of mixing on homogeneity of LENS™ deposited samples.

Completing the development of the LENS™ as a viable tool for combinatorial studies of composition, Collins, et al. [31] implemented the variation in flow rates of powders to affect composition changes in the LENS™. Gradients of Ti-xMo and Ti-xV, both isomorphous β stabilizers of Ti, were deposited by changing flow rates of powders with changes in height of the focused beam. For these studies, one hopper contained pure Ti powder, and the other contained blended elemental powder of composition Ti-25 at%(Mo,V). After ~2mm of material was deposited in the designed cylindrical shape, the flow rates of the different powder feeders were adjusted to deposit a new composition. These depositions were then used to study effects of changing composition on microstructure and properties. By changing composition in incremental fashion, subtle effects of compositional differences can be observed and correlated with microstructure and properties. These studies also began exploring microstructural features and

trend unique to the AM process, such as the steep thermal gradient formed by the melt pool, leading to directional solidification, and long, columnar grain growth perpendicular to the substrate.

Figure 0.10 shows SEM images from this study, showing the transition in microstructure along the composition gradient. All these images were taken along a single prior β grain boundary, which was ~10mm long extending normal to the substrate. Lower concentration of Mo (2.3-7.5 at%) show the typical microstructure of an α/β Ti alloy, with large Widmanstätten α laths growing from the prior β grain boundaries into colony and basketweave type structures. The laths are separated by so called β ribs, which grow thicker with increasing Mo. Above a certain concentration, α laths become small enough to be more aptly described as suspended in a β matrix, as is common of the metastable β microstructure.

Applications and studies of composition gradients with the LENS™

The work outlined above established the LENS™ as a tool for generating a large number of compositions for microstructural study with a previously unheard-of level of efficiency and resolution. Instead of extrapolating from 5 to 10 to 15 wt%, alloy systems can be studied with incremental changes in composition to both discover overlooked aspects of known systems, or rapidly explore entirely new alloy spaces. Two of the more recent and innovative studies done that take advantage of this new tool are discussed. The work of Samimi, et al. [12,32,33] applied this method to the study of the effect of compositional variation on the oxidation resistance of binary titanium alloy systems. Previously, much knowledge about the effect of composition was limited to selected compositions, with large gaps in the compositions space due to cost and time limitations in fabricating a large number of samples to explore each composition in a range.

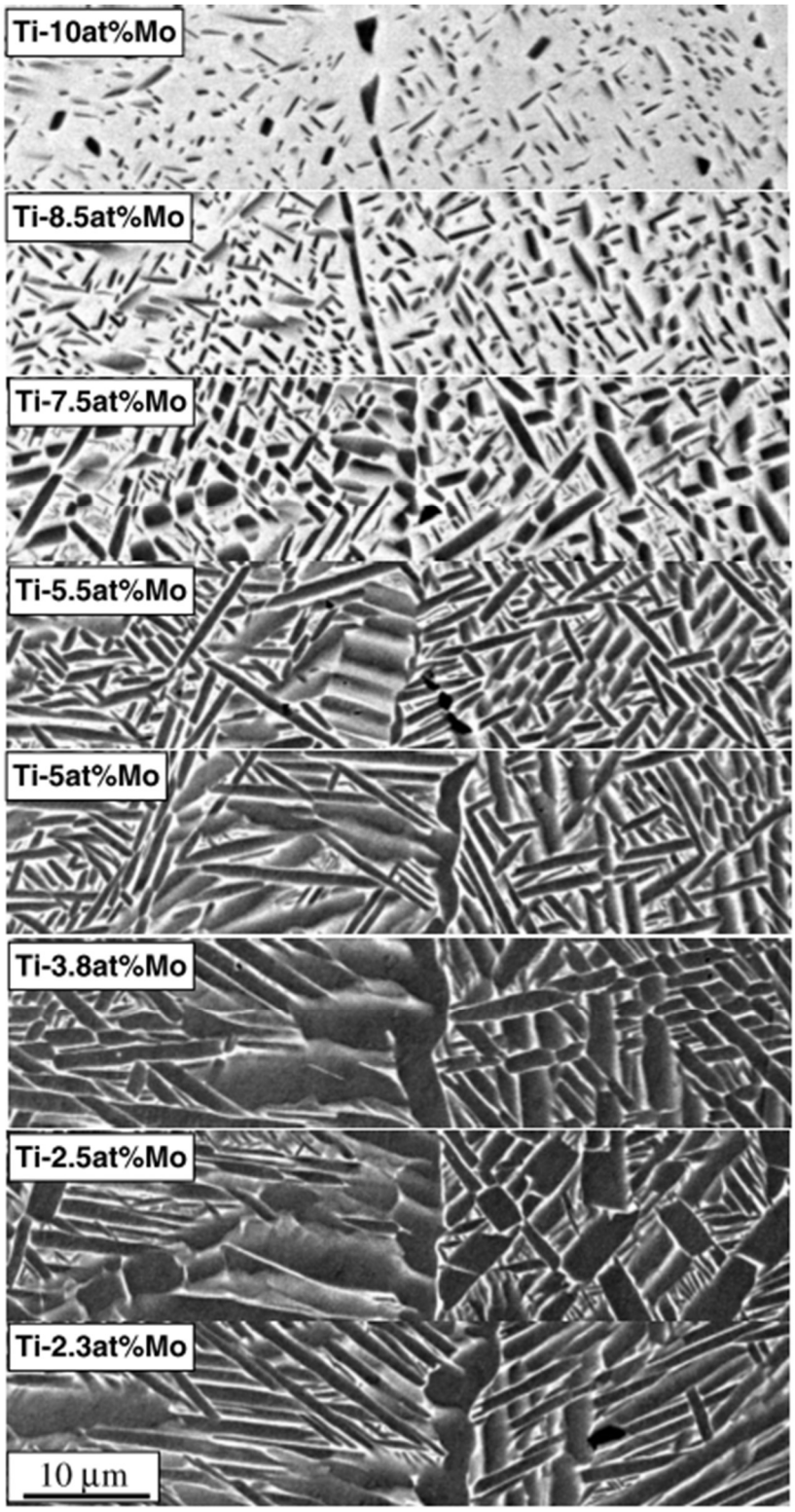

Figure 0.10 – SEM images taken along a single β grain boundary, of a Ti-xMo gradient [31].

Using the LENS™, Samimi was able to explore the effect of increasing alloying element content in single weight percent increments. In the case of the Ti-Cr system, Samimi notes [12] that previous studies had found low concentrations of Cr in Ti (~5 wt%) were detrimental to oxidation resistance, but at higher concentrations Cr was actually beneficial to producing a thin, stable oxide layer. Figure 0.11 shows the results of these studies, where the oxide scale thickness is plotted against the Cr content for samples exposed to still air at 650°C for 25, 50, and 100 hrs.

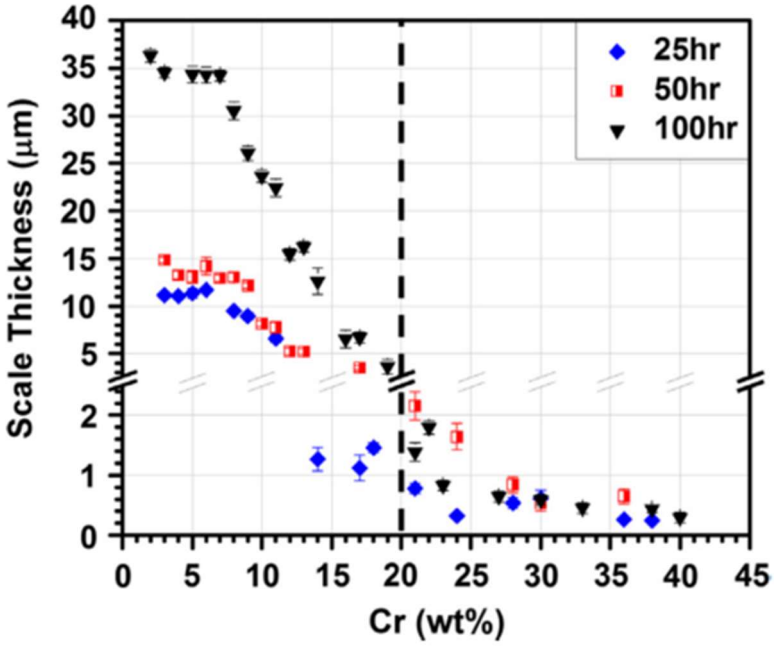

Figure 0.11- Oxide growth in Ti-xCr gradient, for samples oxidized at 650° C.

The results show clearly that above a critical concentration (~20 wt% Cr), the oxide forms a stable layer that resists further growth, and adheres well to the surface of the metal. Samimi attributes the inhibition of further oxygen ingress and oxide growth to the $TiCr_2$ Laves phase, which increases in volume fraction along with the concentration of Cr (Figure 0.12) [12]. At the critical concentration, there is sufficient volume fraction of this phase to prevent further growth in the overall oxide layer. This served as an opportunity to study the oxidation behavior

of titanium alloys beyond simple weight gain. The study of underlying changes in the microstructure and oxide formation gave further insight and information to further control oxidation in metals.

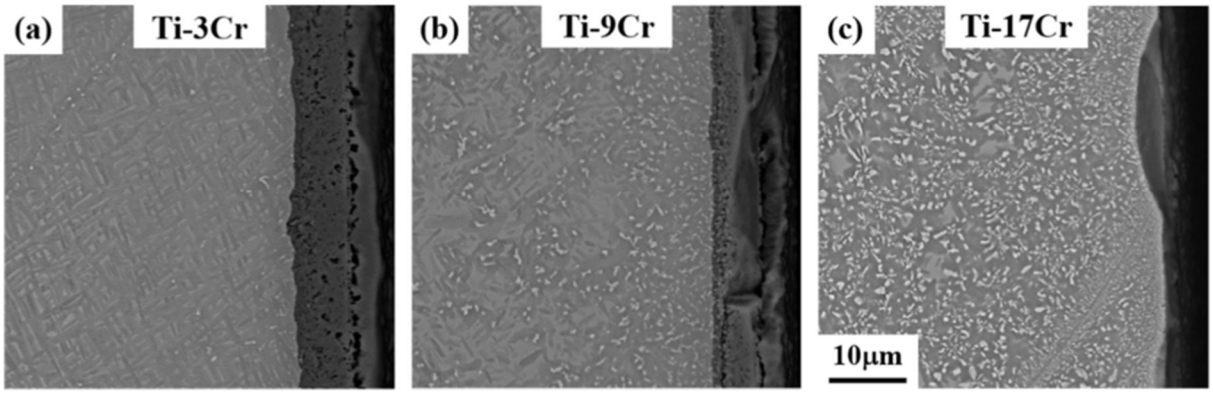

Figure 0.12 - Microstructural and oxide layer changes in Ti-Cr gradient

The LENS^{TM} manufactured composition gradient technique was also used to great effect in work done by Mendoza, et al. [34]. A composition gradient of a binary Ti-(0-30)W wt% system (Figure 0.14) was produced to study solidification and grain refinement in this alloy system. Mendoza applied a model developed to describe the final grain size of a solidified structure in terms of undercooling, density of nucleant particles, and the growth restriction factor Q (Figure 0.14). The additive manufacturing system provided certain advantages over traditional methods of fabrication. The rapid solidification and melting of the LENS^{TM} prevented the mostly immiscible Ti-W from partitioning, as well as provide the ideal thermal gradient in the form of the melt pool for a constant solidification front.

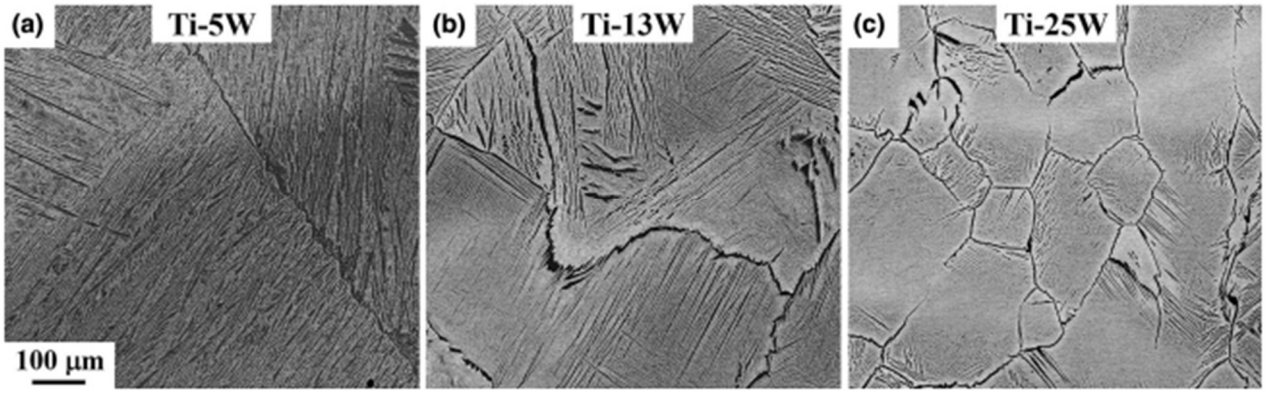

Figure 0.13 – Grain refinement as a result of increasing W in Ti, in a composition gradient made using the LENS^{TM} [34]

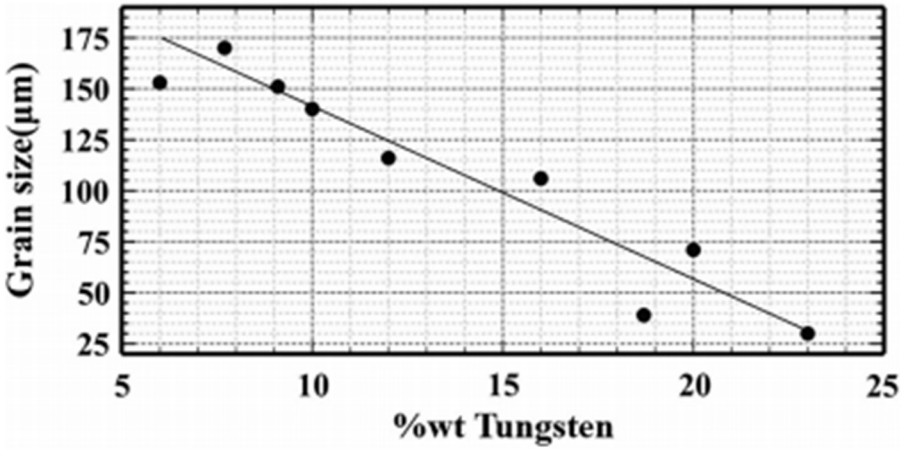

Figure 0.14 – Grain size as a function of wt% W, experimental data vs model [34]

CHAPTER 3. EQUIPMENT AND METHODS

Gleeble Thermomechanical Simulator

The Gleeble Thermomechanical Simulator was developed in the 1980s from systems designed for simulating heat affected zones (HAZ) of welded parts. Since then, the capabilities of the systems offered by Dynamic Systems Incorporated (DSI) have been extended to include all manner of thermomechanical simulations. Forging, hot rolling, swaging, welding, solidification, and flow stress processes can all be simulated on a laboratory scale using the Gleeble. The system couples a resistive heating system, which can heat specimens at rates of up to 1000° C/s, with powerful hydraulics to provide fine-tuned deformation of samples. This is all included in a sophisticated control system which can monitor and control any number of process variables, such as temperature, current, force, position, stress and strain. Thermal control is achieve through welding of thermocouples directly to the surface of the samples to be tested.

Grip choice in the Gleeble

The thermal and mechanical systems of the Gleeble, while impressive on their own, are simply the groundwork for a fully integrated experimental tool. The architecture of the system allows for a great degree of flexibility in both the software control and the hardware of the Gleeble. Figure 0.1 shows the interior of the Gleeble chamber. The wear plates and grips serve as the conduit for the current that heats the sample, which is mounted in the grips. The backing plates serve to secure the grips against the wear plates during testing, also holding the sample in place.

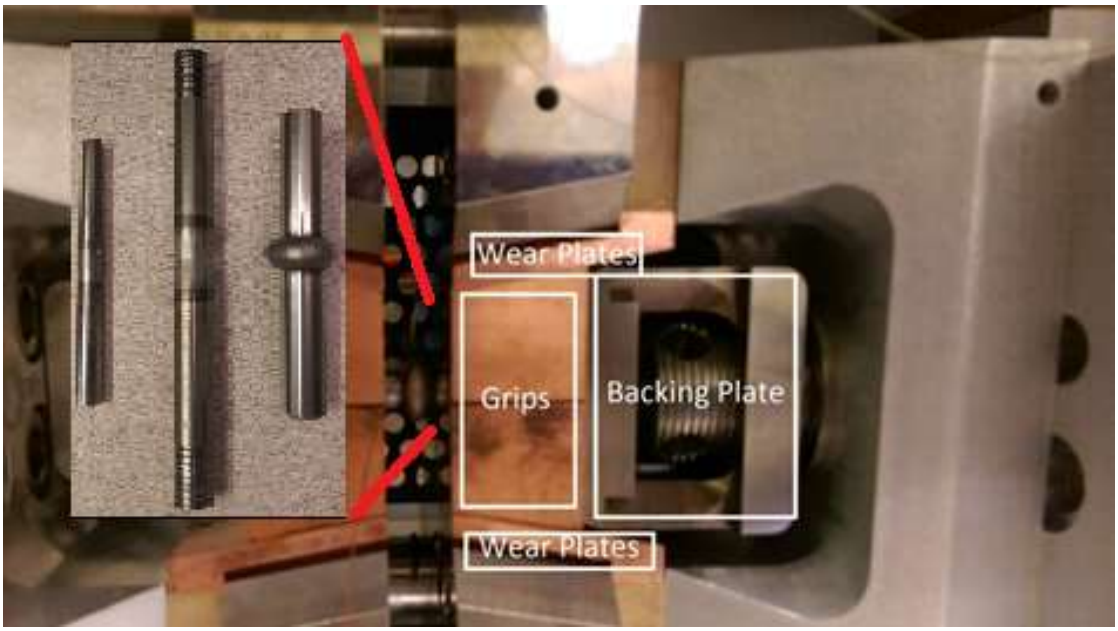

Figure 0.1 - Image of Gleeble jaws, showing interior with round copper grips, a round sample, and compression backing plates. Inset shows some samples post testing, with threaded corresponding to tension and smooth with compression

Choice of grips and backing plates depend on the types of tests being run. The standard grips used in most hot deformation tests are the round copper grips. The copper grips used in the studies described here are designed for 10mm diameter round rods, which must be long enough to span the distance between the two jaws as well as span the length both sets of grips. For tension tests, the samples must have extra threaded length, to secure the samples against the back of the grips. Different sets of backing plates are used in tension or compression tests. The copper grips also afford the tightest thermal control, as the high thermal and electrical conductivity of the grips, combined with the large amount of contact with the test specimen, means that no other setup affords faster cooling and heating capabilities.

Specially designed stainless steel “hot grips” have been used in the studies described here (Figure 0.2). Unlike the copper round grips, these are designed for flat samples up to 50 mm in width, and up to 3.25 mm thick. The low thermal and electrical conductivity of stainless steel,

combined with the minimal amount of grip-to-sample contact, means that heating and cooling of the sample cannot be done at the same speed as the copper grips. No form of mechanical deformation can be done with these grips; they are designed to apply a relatively flat thermal profile across the length of the sample, instead of the steep profile of the copper grips. Figure 0.3, from the Gleeble Operations Manual [35], shows thermocouple readouts along the length of a sample in these different setups. “Hot Jaw” refers to the grips described here, and “Copper Jaw” to the copper round grips. The hot grips are designed to hold a flat, linear, thermal profile across a sample. This linear thermal profile is the starting point for the efforts described in this thesis to design a system to create linear, isothermal, gradient holds on materials for studying thermal ageing on alloys.

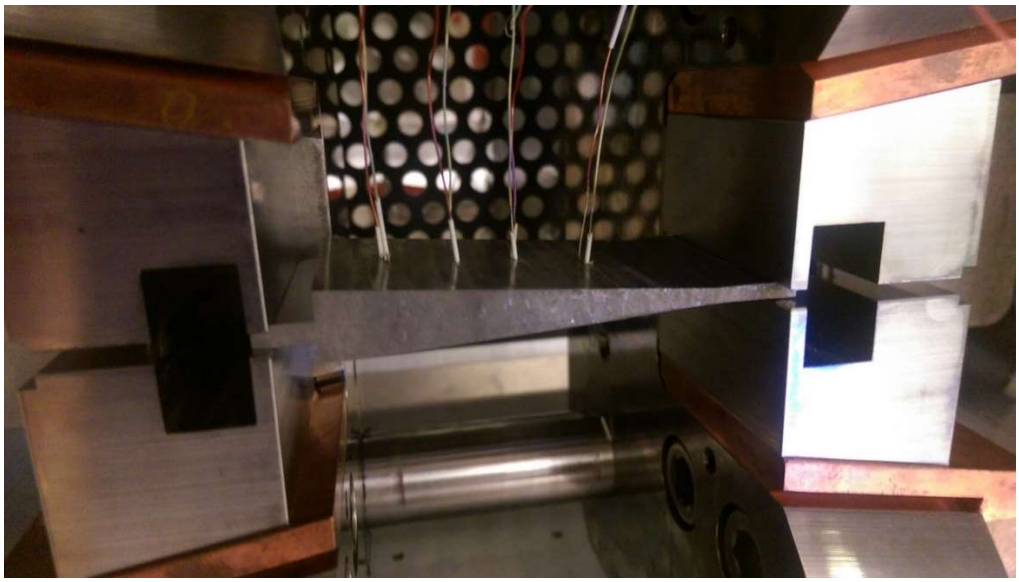

Figure 0.2 – Stainless steel hot grips with flat thermal gradient sample mounted, showing four thermocouples welded along the centerline.

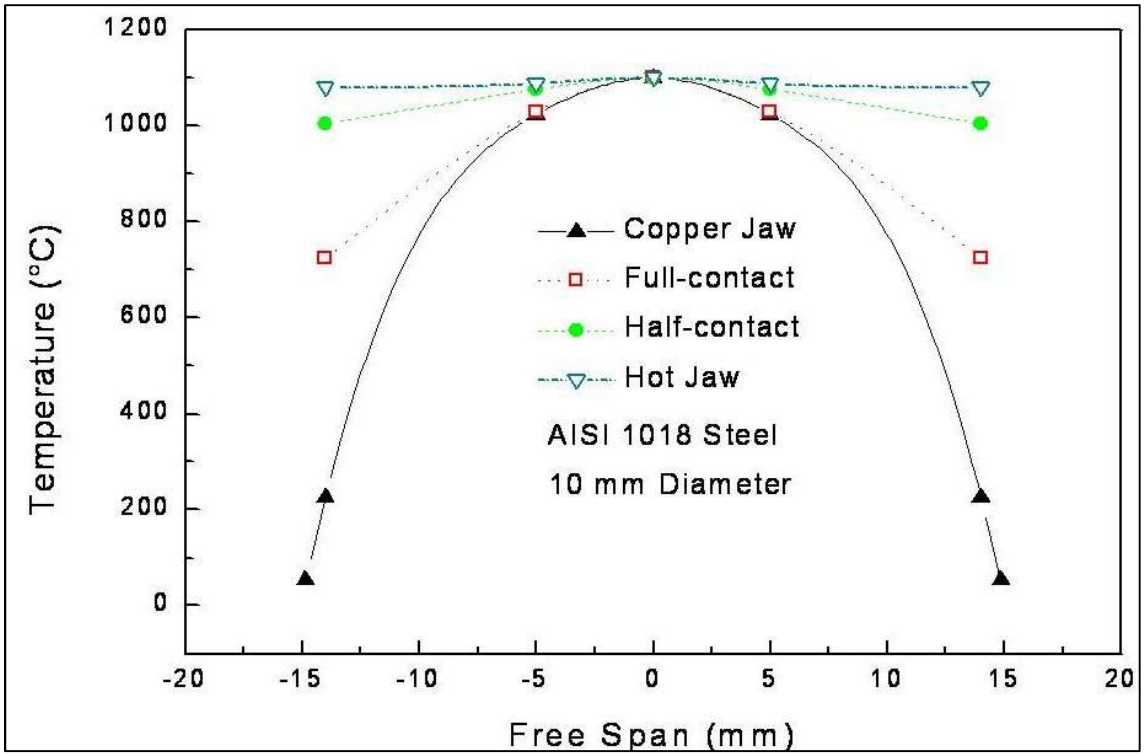

Figure 0.3 - Thermal profiles across samples using various grips in the Gleeble.

Creep testing and strain measurement in the Gleeble

The thermomechanical control of the Gleeble also lead to the development of methods of running rapid, preliminary creep tests in the Gleeble. The load cell of the Gleeble is accurate to the nearest 0.2 kN, so the low stresses required for creep testing (down to 50 MPa) required using the larger gauge size of 10mm round samples. Figure 0.4 shows the sample dimensions used for these tests. After the temperature control thermocouple is welded to the center of the sample, the backing nuts are attached to the threaded section of the sample, and the sample is fitted with the copper grips and inserted in the Gleeble jaws.

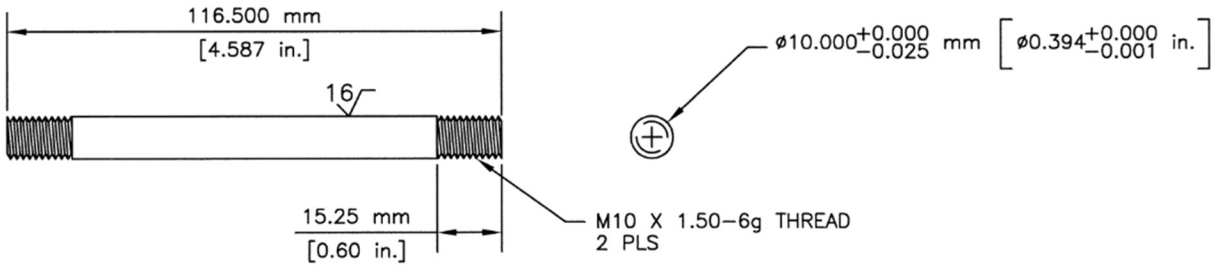

Figure 0.4 – Sample dimensions for tension creep tests in the Gleeble

Strain measurements were done using the DSI supplied 39010 Crosswise-Strain Transducer, or C-Gauge. Figure 0.5 is the C Gauge, with relevant measurement parts visible. The sample is set into the two quartz rods, with the L-rod remaining stationary and the straight rod allowed to move laterally while remaining pressed against the sample surface with a spring. The transducer picks up small lateral movement in the straight rod, which result from changes in the width of the sample. Figure 0.5 also shows clear tubing, which connects to valves in the chamber walls through which compressed air is passed through the body of the C-Gauge to keep the transducer cool during testing. The C Gauge is suspended outside the jaws but inside the chamber, shown in Figure 0.6, centered on the testing specimen and under the thermocouple. After heating of the sample, the C gauge was zeroed in the control software, and resulting changes in position read by the transducer are used to calculated stress and strain in the sample. The Gleeble software give several options for calculating stress and strain; the one used for strain is given in Equation 3, and the one used for stress given in Equation 4.

$$\varepsilon = 2\ln\left(\frac{d_o}{d_o+\Delta d}\right) \qquad \text{Eq. 3}$$

$$\sigma = \frac{Force}{\frac{\pi(d_o+\Delta d)^2}{4}} \qquad \text{Eq. 4}$$

Here, d_o is the initial diameter of the sample, and Δd is the length measured by the C-Gauge.

These equations correspond to radial strain (ε_{rr}), but when discussing uniaxial creep tension tests, axial strain (ε_{zz}) is the norm. Axial and radial stress can be related with Equation 5 and Equation 6, in terms of Young's Modulus, radial strain, Poisson's ratio and polar strain.

$$\sigma_{rr} = \frac{E}{(1+\upsilon)(1-2\upsilon)}[(1-\upsilon)\varepsilon_{rr} + \upsilon\varepsilon_{\theta\theta}] \quad \text{Eq. 5}$$

$$\sigma_{zz} = \frac{E\upsilon}{(1-\upsilon)(1-2\upsilon)}[\varepsilon_{rr} + \varepsilon_{\theta\theta}] \quad \text{Eq. 6}$$

Assuming $\sigma_{rr} = 0$, $\varepsilon_{\theta\theta} = 0$, and substituting $\sigma_{zz} = E\varepsilon_{zz}$, this becomes Equation 7.

$$\varepsilon_{zz} = \frac{\upsilon}{(1-\upsilon)(1-2\upsilon)}\varepsilon_{rr} \quad \text{Eq. 7}$$

Assuming a poisson's ratio of, $\upsilon = 0.3$, the equation becomes $\varepsilon_{zz} = 1.3\varepsilon_{rr}$, which was used in all studies to convert given radial strain to axial strain. The creep tests were done to compare results with previous work in generating Larson-Miller plots. Thus, the tests were set up to run such that the 0.2% strain point could be determined.

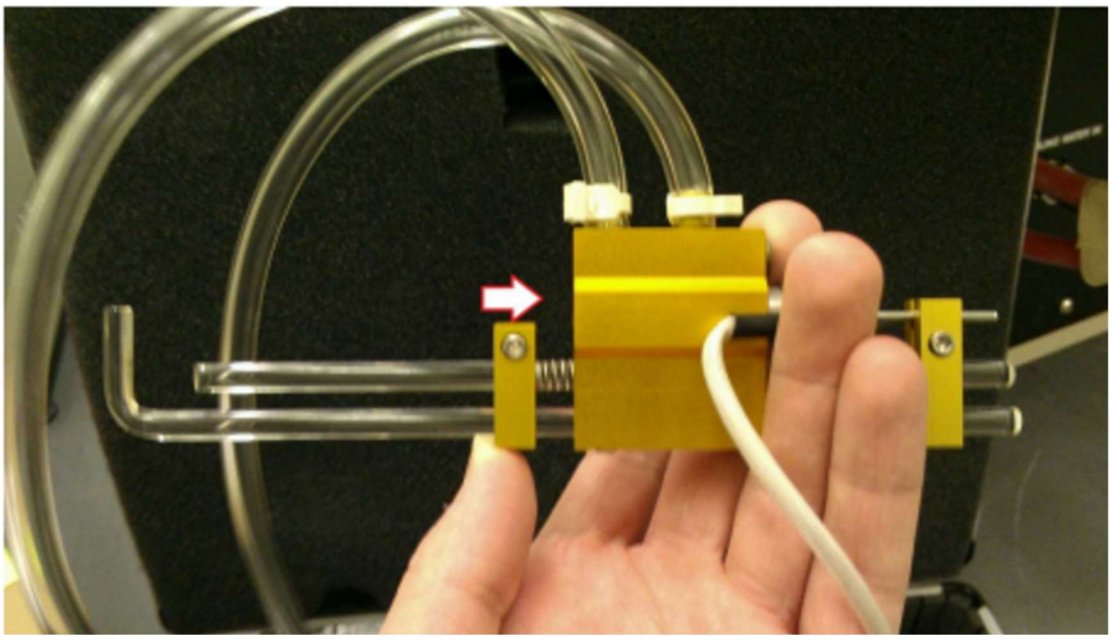

Figure 0.5 – DSI 39010 Crosswise-Strain Transducer (C-Gauge) showing quartz rods, transducer housing, and cooling tubes [35].

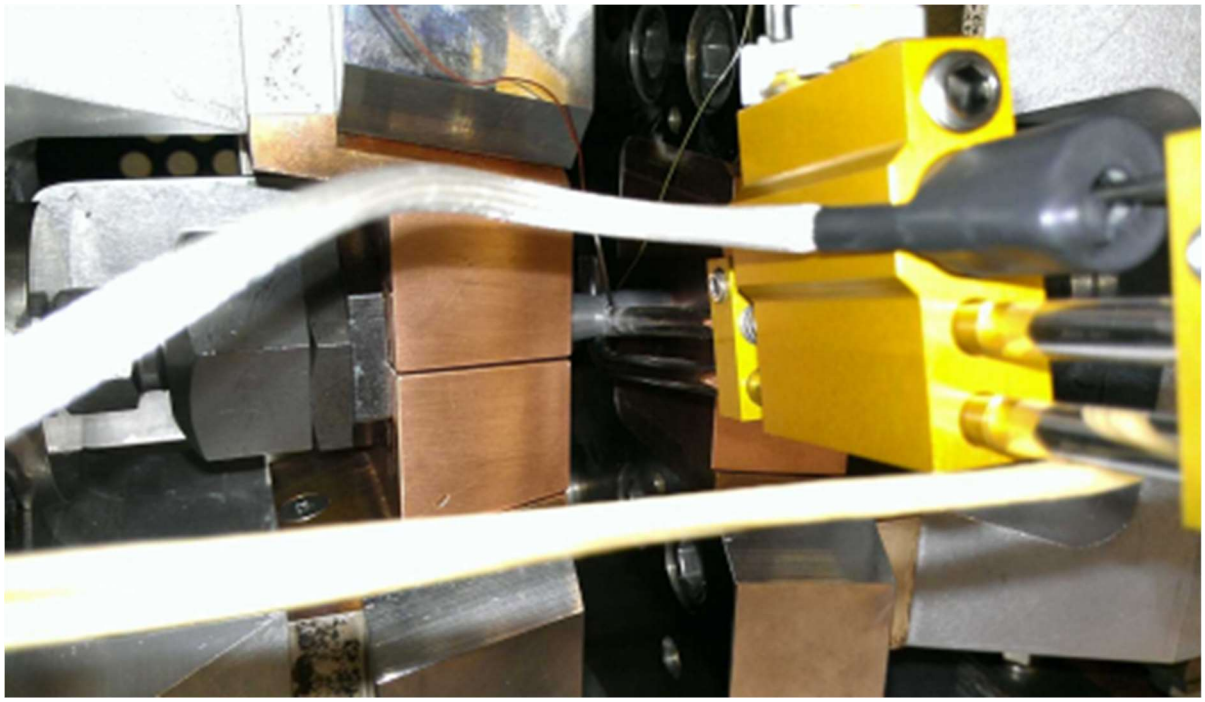

Figure 0.6 – C-Gauge hooked up to a 10mm diameter tension sample [35].

Rapid Alloy Fabrication using LENS™

The Optomec Laser Engineered Net Shaping (LENS™) system at the Ames Laboratory Materials Preparation Center (MPC) was used for the fabrication of compositionally graded samples. The LENS™ is a laser melted, powder blown Additive Manufacturing system, where metal powder is blown into a melt pool generated by a laser, which moves along to generate a 3D shape specified with a CAD model.

Composition gradients in the LENS™

The LENS™ MPC has four powder feeders, which allow for several different powder compositions to be directed simultaneously. The movement of the powder head of the LENS™ is directed by a Digital Motion Control (DMC) file, which is a human readable text file that encodes information for the x y motion of the head, and z motion of the build plate. This can be edited manually to encode other commands into the automatic control. In this study, the files were edited to affect a change in the ratios of the different powder feed rates from the respective powder feeders, and change the composition generated in a single build.

Typically, the powder feed rates are changed when there is a change in layer, so the bottom of the build starts with 100% of the powder coming from one powder hopper, and the top of the build has all the material built from another hopper. Given the nature of the process, where layers are remixed with each other through subsequent passes and remeltings, it is wise to build several layers of a certain composition before moving on to the next composition. For all composition gradients fabricated for this study, the composition was changed every seven layers. The sum of all the powder feed rates should be held constant throughout the build, otherwise there could be overbuilding or underbuilding.

Elemental powder usage

While prealloyed powders would lead to better compositional homogeneity, the goal of this work is to provide a framework for rapid, cost effective and flexible alloy study and development. Elemental powders were weighed and mixed to achieve the desired compositions. These were weighed out using an OHAUS digital scale to 0.1 g. The powders used, and the relevant data on the powders given by the manufacturers, is given in Table 0.1. The relevant

alloy compositions were loaded in Nalgene bottles, and mixed with a Turbula T2C mechanical mixer for 20 minutes to ensure good mixing.

Table 0.1 – Manufacturer parameters for elemental metal powders used

Element	Manufacturer	Purity	Mesh Size/ Powder Type
Ti	Alfa Aesar	99.9%	-150
Cr	Alfa Aesar	99.99%	-100/+325
Al	Alfa Aesar	99.97%	-100/+325
Nb	Wah-Chang	99.9%	-100/+325
Si	Atlantic Equipment Engineers	High Purity	Plasma Spray Grade

Of concern when designing the builds is the issue of blended powder composition versus final part composition. Several factors can lead to mismatch between the two. A large disparity in size between the powders can lead to self-segregation, and the composition of the blown powder can change as the build continues. Thermodynamic factors can lead to certain elements being rich or poor in the final build. Peterson observed that when deposited with Ti, especially at higher compositions (>10 wt%), the higher density, higher melting temperature, and low heat of mixing of Mo and W lead them to be poor in final composition. Likewise, the low melting temperature, high exothermic mixing, high density and low reflectivity of Sn meant that deposits with Sn came out extremely Sn rich [20]. Peterson compensated by increasing Mo and W by 1.3, and decreasing Sn by 0.3. Al, Cr and Nb have also been known to appear in lower concentrations printed than in powder when mixed with Ti.

Processing parameters and energy density

LENS^{TM} process variables of laser power, hatch width, layer spacing, and beam head travel speed are all important parameters to achieve a fully dense, compositionally homogenous part at the end of the process. As discussed in Chapter 2, this is especially relevant when using blends of elemental powder, where alloying is done in situ, as thermodynamic factors of enthalpy of mixing and melting temperature must be considered. These processing parameters are frequently combined into a single energy density term. Table 0.2 gives the build parameters used in this study. Note the significant increase in energy density required in the samples containing Nb, which has both high melting temperature and enthalpy of mixing with Ti, even in small amounts. Depositions also changed hatching patterns after each layer, changing by 45° each time.

Table 0.2 – Build parameters for LENS^{TM} depositions

	Hatch Width	**Layer Height**	**Travel Speed**	**Laser Power**	**Energy Density (kJ/in^3)**
Ti-Cr-Al-Nb-Si Oxidation	0.015”	0.01”	25 ipm	330 W	1.5
Ti-Cr Wedge	0.015”	0.01”	40 ipm	330 W	0.9
Ti-Cr-Al-Nb-Si Wedge	0.015”	0.01”	27 ipm	390 W	1.6

Oxidation tests using LENS^{TM}

The oxidation tests done used the same methods described by Samimi [12,32,33]. First, a composition gradient is selected for investigation, and a 7mm x 7mm square pillar is printed in

the LENS™ with a composition gradient using the techniques described here. Figure 0.8a shows an example of one of these depositions used for oxidation study. The resulting compositionally graded sample is removed from the plate, β solutionized at an appropriate temperature for 20 minutes to homogenize the microstructure, and then sliced down the middle with a low speed diamond abrasive saw. The cut face is ground using silicon carbide paper, and polished to 0.02 μm colloidal silica to provide a clean, smooth surface for oxide to grow. The polished faces are then left exposed in still air at 650° C for 25 and 100 hours, respectively. These were then mounted and polished such that the oxide scale could be imaged along the composition gradient. Figure 0.7 shows the geometry of the final imaging surface of the sample, to see the surface that is imaged perpendicular to oxide layer. In this way, the oxide layer can be examined as it changes with composition, along with microstructural changes moving from the oxidized surface into the bulk of the sample.

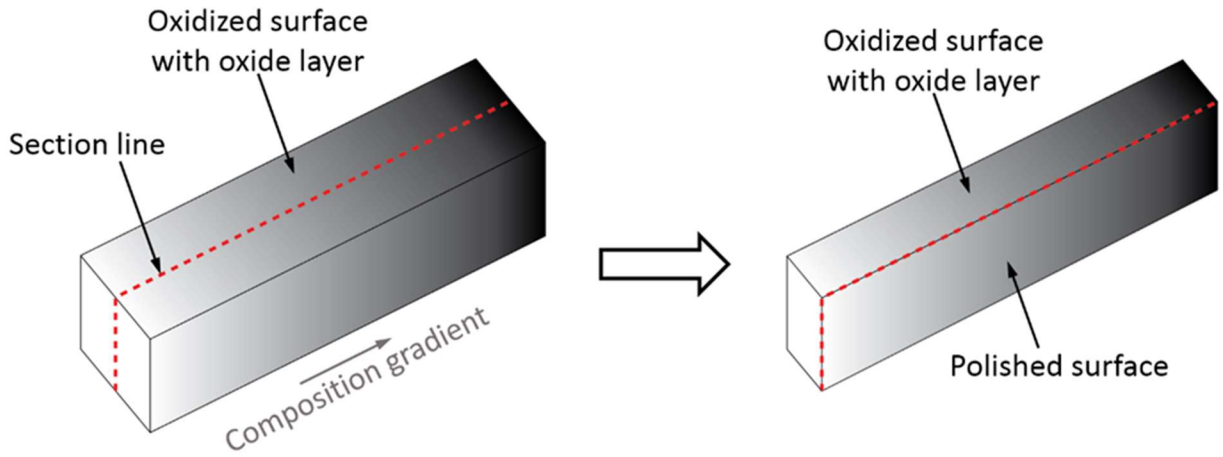

Figure 0.7 – Oxidized sample, showing imaged surface perpendicular to oxide layer and composition gradient [33].

Near net shaping capabilities for thermal gradient samples

While one major advantage of additive manufacturing technology is the ability to create a wide variety of 3D shapes in short amounts of time, this capability has not been utilized in the context of LENS^{TM} built composition gradients. This has changed with the development of the thermal gradient method described in Chapter 4. Samples can be printed with a composition gradient from top to bottom, in the shape required for the application of the thermal gradient; the result is a sample with perpendicular gradients of process variables, allowing for the exploration of a complete range in both directions. Two such samples were produced and studied microstructurally for this work: a Ti-(0-15)Cr (Figure 0.8b) and Ti-10Cr-3Al-(2-6)Nb-(0.2Si-0.6)Si.

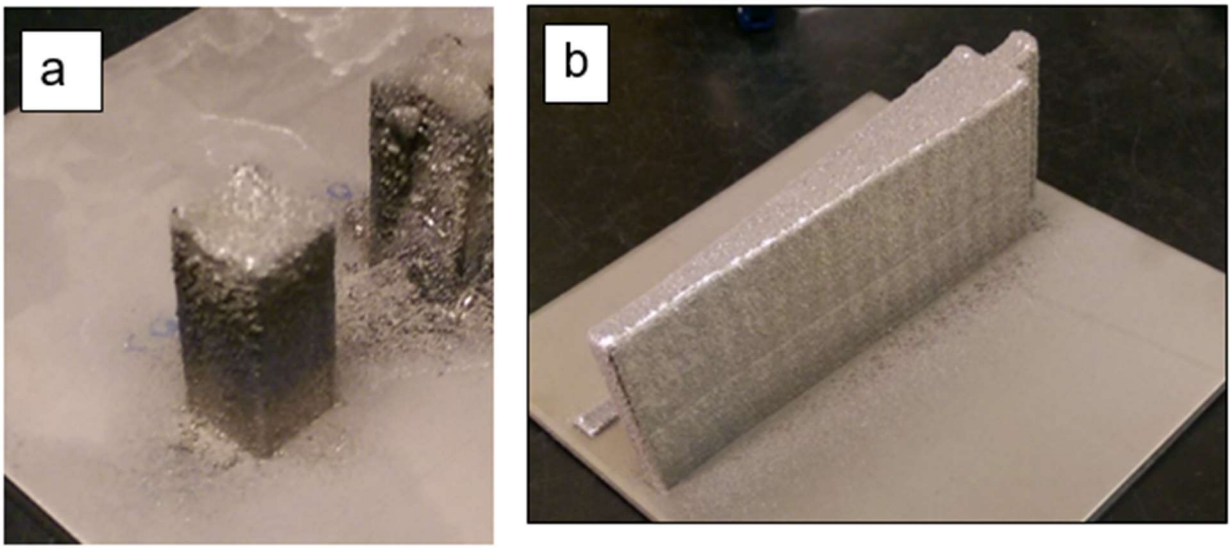

Figure 0.8 – Compositionally graded LENS^{TM} depositions for a) oxidation study and b) bicombinatorial microstructural study

Finishing, solutionization and ageing treatments of bicombinatorial specimens

While the LENS^{TM} does achieve good near net shape, surface finish is poor. Final machining is required to ensure the desired final shape, with flat surface finish for good contact with the Gleeble grips, even heating of the sample, and carefully controlled cross sectional area.

This is especially relevant in the regions gripped by the Gleeble grips, and the area where the thermocouples are attached. The CAD file used to print the gradient samples was made 1mm thicker on all sides, to allow the final shape to be machined out. Machining of the final shape from the printed specimen was done by the Iowa State University Chemistry Machine Shop.

Ti samples produced via the LENS^{TM} for microstructural study are typically β solutionized before any subsequent thermal treatments are done. This serves to homogenize the microstructure, as well as provide a known starting point for further investigation. In the case of the Ti-Cr binary gradient, it was desired to transition from the β solutionization temperature (~935° C) directly to the ageing range (700°-600°). This is because upon quenching from the β phase field below ~200° C, Ti can form the athermal ω phase [1]. This phase can serve as a nucleation point for α, and introduce further variables in the experiments. While ω has been exploited to produce fine scaled α precipitates [36], here it was to be avoided. In order to ensure all portions of the gradient were above the 935° C mark, certain sections of the specimen would be held at temperatures in excess of 1200° C. Type K thermocouples used here not only have an accuracy limit of ~1000° C, but do not stand temperatures much above that and will detach from the sample. Effort was made to better secure the thermocouples to the surface, but ultimately, a different approach was taken. First, the sample was taken up to the ageing temperature with all four thermocouples attached and allowed to come to steady state, and the thermal profile was recorded. Then, the sample was brought down to room temperature and the three thermocouples corresponding to the hotter portions of the sample were removed. The control thermocouple, in the thickest, coolest part of the specimen, was left in place. This was set to bring the sample up to the solutionization temperature, knowing all other points of interest would be well above the solutionization point, while maintaining thermal control. By recording the steady-state ageing

temperature before solutionization, when the control thermocouple was brought to the ageing setpoint the thermal profile was already known with a single control thermocouple. Figure 0.9 shows a schematic of this thermal history, and Figure 0.10a shows the Ti-Cr sample after ageing.

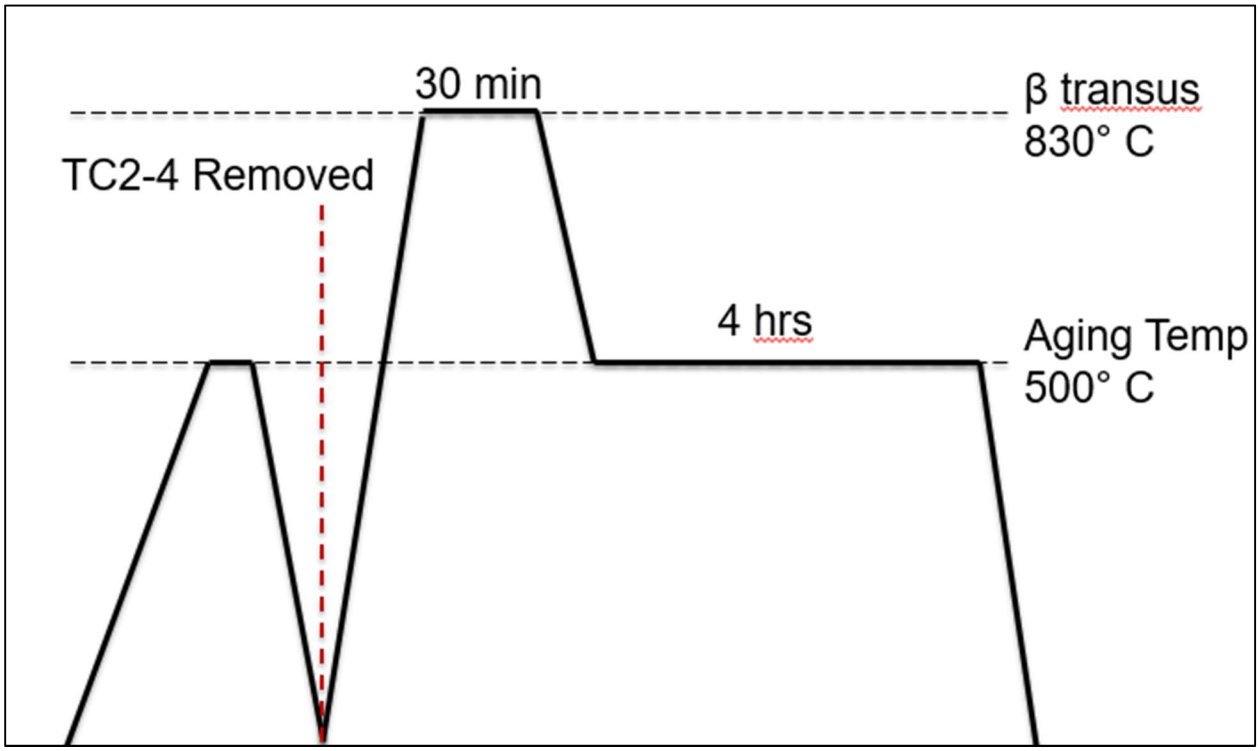

Figure 0.9 – Thermal history of control thermocouple (TC1) for Gleeble solutionization and ageing.

Characterization of bicombinatorial samples

For the bicombinatorial samples, a major benefit is the ability to track subtle changes in microstructure in two dimensions. Thus, sectioning of the final aged part was to be avoided. The EDM at the Ames Lab machines shop was used to cut the entire length and height of center plane of the sample. Electrical discharge machining (EDM) is a technique that utilizes a high voltage wire to tear away atoms from conductive materials and create no microstructural deformation or residual stresses in the material. In effect, the “wings” seen in Figure 0.8b were sectioned off,

leaving only the rectangular flat plate underneath. This sample, being much too large to hand polish or utilize traditional metallographic mounts, was instead super glued to stainless steel "dummy" pucks that could fit in the polishing head of a Buehler Automet 2000 autopolisher. The sample was ground with silicon carbide grinding pads, and polished to 0.04 μm colloidal silica. The polished sample was etched using Kroll's reagent for optical imaging Figure 0.10b, and subsequently repolished for SEM imaging. SEM imaging was done at the Materials Analysis and Research Lab (MARL) at ISU, using a FEI-Quanta 250 FE-SEM.

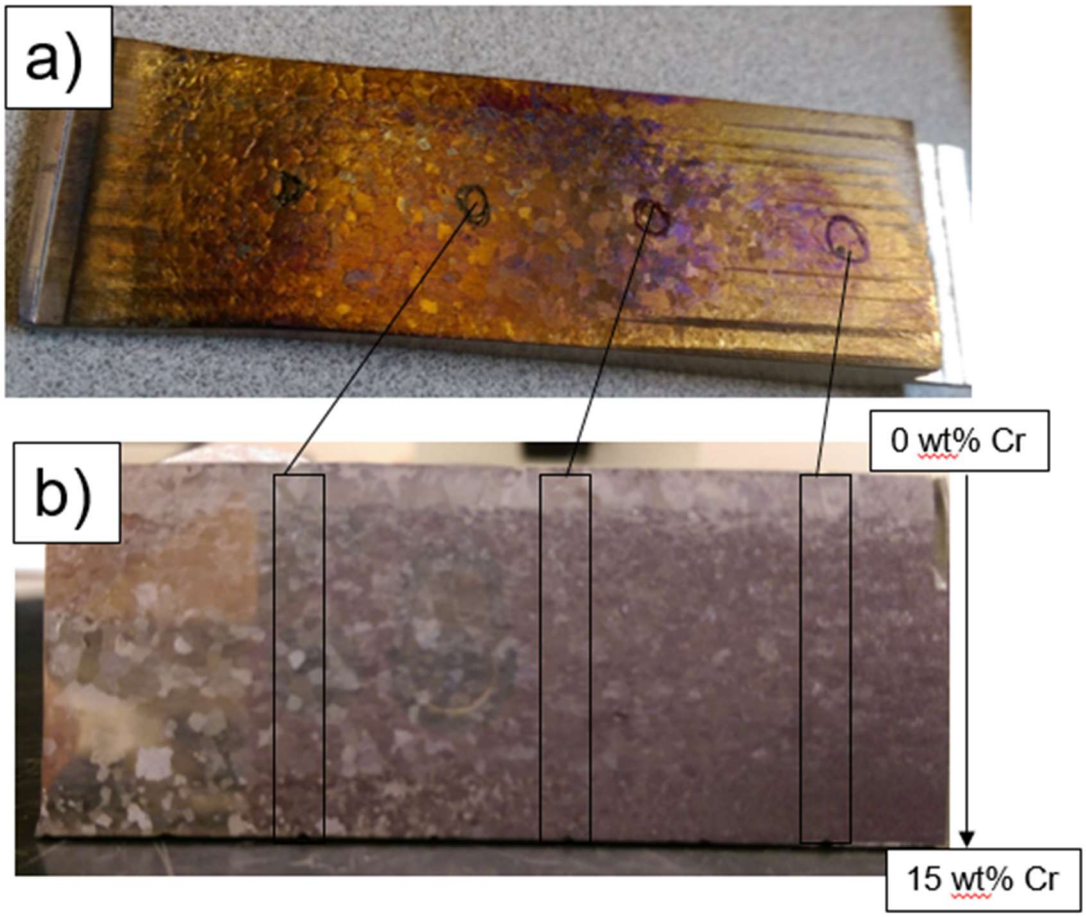

Figure 0.10 – a)Ti-Cr bicombinatorial sample after ageing. b) Ti-Cr sample after EDM extraction, polish and etch.

Creep Specimen Preparation

Machining and ageing

A plate of β-solutionized β-21S was obtained from Timet, and used in both the thermal gradient development, and baseline creep studies in the Gleeble. 10mm rods were extracted from the plate by the Ames Lab machine shop using EDM, and subsequently machined according to the specifications in Figure 0.4. For ageing treatments, the samples were encapsulated by the Iowa State University Chemistry Department Glass Shop in quartz glass along with Ti sponge to act as an oxygen getter (Figure 0.11). The tubes were vacuumed, and backfilled with argon to further reduce oxidation of the samples during ageing.

Figure 0.11 – Rods encapsulated in quartz glass, with argon atmosphere and Ti sponge

Drop casting of select composition

After rapid characterization and screening of select alloy compositions and ageing temperatures, specimens for creep testing were fabricated at the Ames Lab Material Preparation

Center (MPC). Alloy of the requisite composition was arc-melted into buttons, and subsequently drop cast under argon atmosphere (Figure 0.12). They were machined and heat treated using methods described.

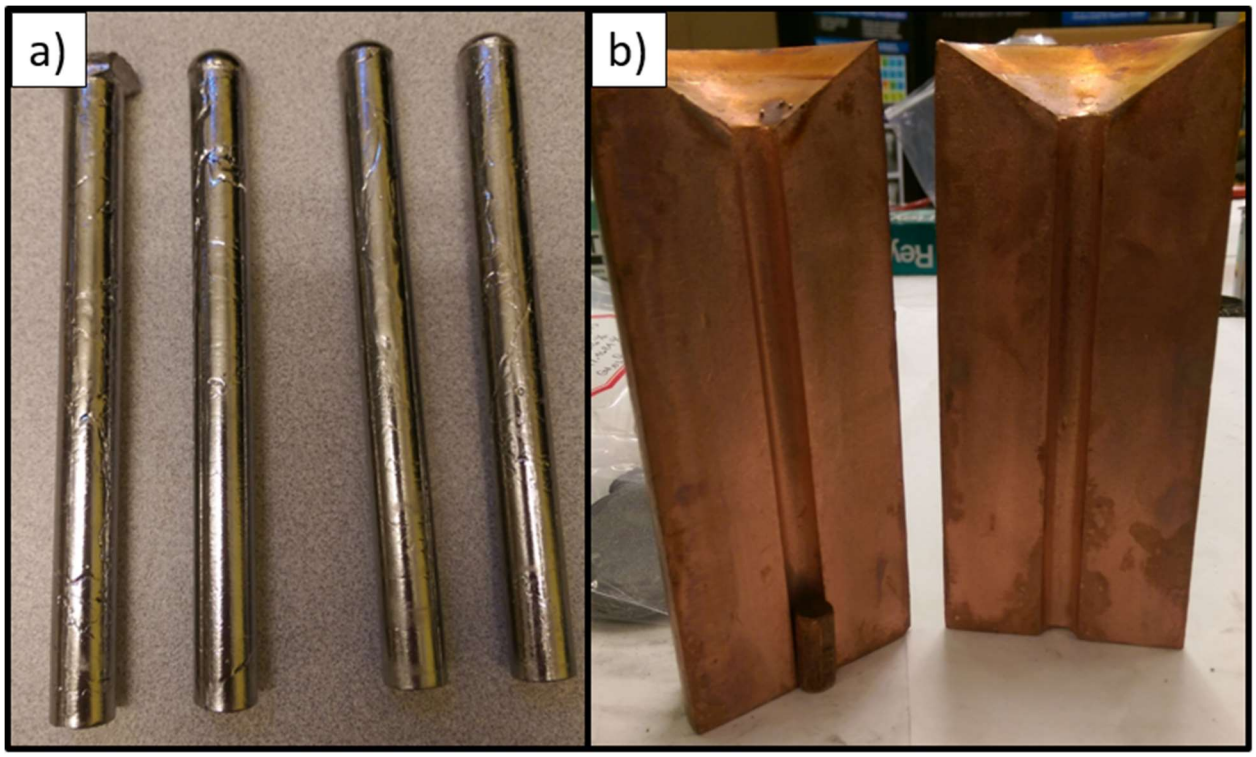

Figure 0.12 – a) Arc melted and drop cast 11mm diameter samples b) Water cooled copper split molds used for drop casting arc-melted buttons.

CHAPTER 4. ENGINEERED, SPATIALLY VARYING ISOTHERMAL HOLDS: ENABLING COMBINATORIAL STUDIES OF TEMPERATURE EFFECTS, AS APPLIED TO METASTABLE TITANIUM ALLOY β-21S

A paper published in Metallography, Microstructure and Analysis
Figures renumbered to match the rest of the thesis

Brian Martin[1,2,*], Peyman Samimi[1,2], Peter Collins[1,2,3]
1: Department of Materials Science and Engineering, Iowa State University, Ames, IA 50011
2: Center for Advanced Non-Ferrous Structural Alloys, an NSF I/UCRC
3: Ames Laboratory, Iowa State University, Ames, IA 50011

Abstract

A novel method to systematically vary temperature and thus study the resulting microstructure of a material is presented. This new method has the potential to be used in a combinatorial fashion, allowing the rapid study of thermal holds on microstructures to be conducted. This is demonstrated on a beta titanium alloy, where the thermal history has a strong effect on microstructure. It is informed by simulation, and executed using the resistive heating capabilities of a Gleeble 3800 thermomechanical simulator. Spatially varying isothermal holds of 4 hours were affected, where the temperature range of the multiple isothermal holds varied by ~175°C.

Introduction

In recent years, there has been an increasing use of combinatorial approaches for exploration and evaluation of alloy systems [12,37,38]. In this context, “combinatorial” refers to the production of samples across a wide range of processing parameters or compositions to rapidly optimize for desired properties. For example, the fabrication of compositionally graded Ti-xM systems using binary powders and powder based additive manufacturing systems allows

for study of the effects of composition on properties such as high temperature oxidation resistance [12,37] or phase transformations [38]. This combinatorial approach has proven beneficial because it allows for the simultaneous assessment of large numbers of compositions (often at a fixed thermal history) without the need to produce large numbers of samples, consequently cutting the time and effort required to study the effect of composition on microstructure, properties, and performance. One of the oldest combinatorial approaches (though not identified as such) is the Jominy End Quench Test [39] which allows for rapid studies of the effect of the cooling rate on microstructure and properties. Isothermal gradients and their effects have also been studied. The affect of the heat affected zone (HAZ) in welds is one of the oldest examples of this, and still a topic of study [40]. In these cases, the HAZ is an uncontrolled, short term heating, rather than any sort of tailored thermal gradient. Methods have been developed to induce thermal gradients via even heating in a traditional furnace, and then cooling at one end to induce a thermal gradient [41,42]. These techniques have been adapted to vary properties in forged nickel based superalloy turbine disks [43,44]. These studies clearly show the influence of uneven thermal exposure, but are often concerned with the resulting microstructure in the finished, full sized part, with thermal monitoring limited to a few points, as well as a nonlinear thermal profile across the sample. The microstructural variation is also of note, in that the recrystallization post forging is often the focus, where larger grains are desired in the outer rims, and smaller grains in the bore region [43,44]. In these studies, there is a sudden change in microstructure as the temperature threshold for recrystallization is crossed, rather than a gradient in features and properties to follow with the gradient in temperature. They also rely on heat flux alone, rather than any uneven heat source. While these techniques allow for the study of variations in cooling rate and aging temperature, the ability to engineer and affect thermal

gradients comprised of isothermal holds in a systematic, controlled and small scale would provide a way to study more closely these thermal gradients. This is difficult to do, and is rarely conducted owing to an absence of an instrumented technique to control such gradients of variable temperature isothermal holds. Presented here is an extension of these combinatorial approaches for the creation of a controlled temperature gradient within a single sample over a length scale larger than the attending microstructural features, such as grains and precipitates.

Methods and Materials

The novel use of a Gleeble system enabled the application of a temperature gradient onto a single sample, where a 200° temperature gradient can be held for a lengthy period of time. Manufactured by Dynamic Systems Inc. (DSI), the Gleeble is designed to perform a wide variety of physical simulations of thermomechanical processes [45]. The Gleeble 3800, which was used for these tests, has the capability of heating and cooling samples at highly controlled rates, all in the presence of an inert atmosphere or vacuum. The instrumented experimental technique was informed by finite element software, in the form of COMSOL Multiphysics, and the microstructure quantified using relatively new methods of quantification, namely MIPAR™, to demonstrate this new method for rapid evaluation of isothermal holds on alloy systems.

TIMETAL 21S, or β-21S, is a metastable beta titanium alloy developed for oxidation and corrosion resistance for use in aerospace applications [5]. Like all metastable beta alloys, β-21S retains its high temperature β *bcc* (body centered cubic) structure when quenched from above its beta transus of 807° C. The alloy must be aged below its beta transus in order to precipitate out the low temperature α *hcp* (hexagonal close packed) phase to strengthen the material [1]. The exact size and distribution of these alpha precipitates strongly influence the mechanical properties, and are very sensitive to the aging temperature and time [1,36,46]. β-21S is an ideal

candidate alloy for verifying the novel experiment proposed here. When this alloy is exposed to a thermal gradient, a corresponding variation in microstructural features such as volume fraction of phases and feature size (e.g. α laths) would be expected. A plate of β-21S (~38mm thick) in the fully beta solutionized condition was provided by Timet and was used to demonstrate this new technique. The nominal chemistry of this plate, performed by Timet, is given in Table 0.1.

Table 0.1 – Chemistry given by TIMET for β-21S plate used in thermal gradient study.

Element	Mo	Nb	Fe	Si	Al	C	O	N	H (ppm)
Wt%	15.0	2.6	0.3	0.21	3.1	0.02	0.14	0.01	83

Results and Discussion

The known phenomenon of resistive heating is the basis for this technique. The basic relationship between current (I), power (P), and resistance (R) is given in Eq 1.

$$P \propto I^2 R \qquad \text{Eq.1}$$

In physical simulators, such as the Gleeble, where resistive heating is used to heat the specimen, the current remains constant across the length of a single piece of material. Consequently, by varying the cross sectional area, and thus the resistance, the conversion from electrical energy to heat energy in that area will vary in a predictable way, allowing the Gleeble to be used as a controlled, resistive thermal gradient unit. Thus, this technique requires some sort of controlled resistive heater.

The objective of the research work is to affect an approximately linear temperature gradient with a temperature change of ~200° C across the sample. The Gleeble stainless steel hot grips were used for this study, as they not only allow for the usage of a flat sample, but also

induce a more uniform thermal profile when compared with the sharper thermal profile of the more standard round copper grips [35]. The concept of the experiment was further explored using a finite element modeling approach to account for heat flow, radiation loss, and non-uniform conductive heating. Specifically, COMSOL Multiphysics was used in an exploratory manner to assess the approximate dimensions and shapes required to achieve the aforementioned criteria. Current, joule heating, and heat flow were included in the bulk sample, and boundary conditions were set for where the Gleeble grips would contact the sample on the surface. These boundary conditions had the relevant voltage drop across the sample, as well as room temperature conditions at the point of contact, to approximate the cooling of the grips.

A sample of β-21S was cut and machined to the final geometry (Figure 0.1a) from the beta solutionized plate for the verification of the proposed technique. Four K-type thermocouples were welded to the surface of the machined sample for the purposes of monitoring and controlling the temperature along the sample, as marked in Figure 0.1a. To avoid oxidation on the sample, the Gleeble test chamber was rough pumped and backfilled with argon 3 times, then diffusion pumped to $2.6*10^{-5}$ torr. The controlling thermocouple was positioned at the narrowest point, where the temperature would be the highest. The controlling set point of this position was 700° C. Given that the stainless steel grips do not allow for the same rapid ramping up of temperature that the copper grips do, the sample was heated over three minutes. The other three thermocouples were allowed to come to temperature, and monitored to determine when the temperatures reached a steady state (Figure 0.2). The specimen was held at the spatially graded isothermal holds for four hours to allow the microstructure to reach a reasonable degree of equilibrium.

Following the Gleeble experiment, the sample was cut along the center line, cold mounted and polished with 0.04 μm colloidal silica as a single piece, and imaged using an FEI Quanta 250 FE-SEM in backscatter mode. Images were taken along the points where the thermocouple was taking direct measurements, shown in Figure 0.3. This was done simply to verify that the expected variation in microstructure followed the change in aging temperature. As expected, there was a marked variation in the microstructure as the aging temperature increased from 527 to 700° C. As the temperature increased, the alpha phase stability drops, and the

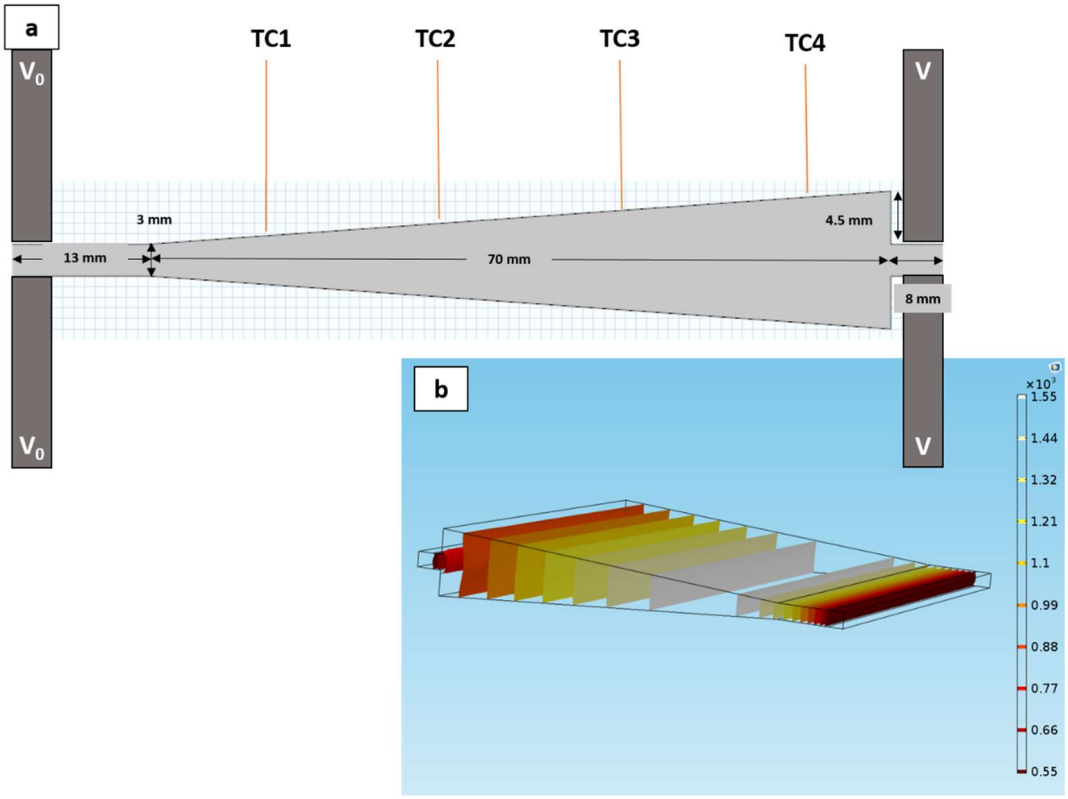

Figure 0.1 - (a) Schematic of the experimental design, showing dimensions of the sample, location of thermocouples, and points of contact for the grips, which provide current as well as cooling. (b) Graphic of the COMSOL model, showing the isothermal surfaces, perpendicular to the current flow.

volume fraction of alpha naturally declines. A quantitative analysis of the volume fraction of the α phase at various points was done using MIPAR™, a new and powerful image processing

software package [47]. Using adaptive thresholding, MIPAR^{TM} is able to automatically differentiate features in an image for quantification, and apply the same procedures automatically to an entire batch of images for rapid acquisition of a large amount of microstructural data. As expected, the volume fraction of alpha declines with increasing temperature, and the microstructure transitions from a refined basketweave microstructure consisting of interpenetrating α laths, to coarse, discrete α particles dispersed in the β matrix. Usually, the finer scaled α phase is desired for the increased hardness and strength, and much work has been done to engineer finer scale structures in β-21S[36,48]. To show this change in in mechanical properties across this therally graded sample, a rudimentary assessment was conducted by measuring the Vickers microhardness at the four points of interest. A summary of these characterization efforts is presented in Table 0.2.

Table 0.2– Hardness and microstructural quantification of gradient aged β-21S

	X (mm)	T (°C)	Hardness	Volume Fraction α
A	9	700	298.1 ± 6.1	0.27 ± 0.04
B	25	673	329.4 ± 12.1	0.37 ± 0.04
C	43	604	369.8 ± 8.4	0.52 ± 0.03
D	60	527	442.2 ± 10.6	0.62 ± 0.05

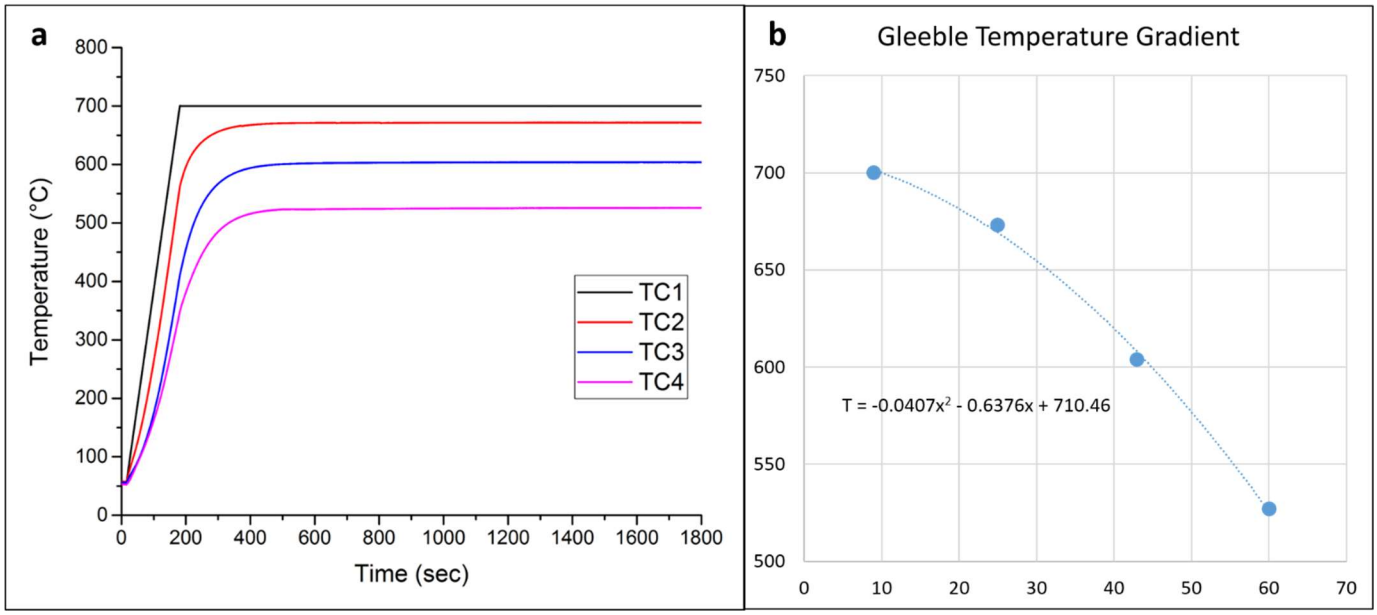

Figure 0.2- Thermal data, taken from the thermocouple readouts on the Gleeble.(a) Plot of thermocouple readouts, showing the heating of the sample and the steady state temperatures. (b) Plot of the steady state temperatures along the length of the sample, fitted to a quadratic function.

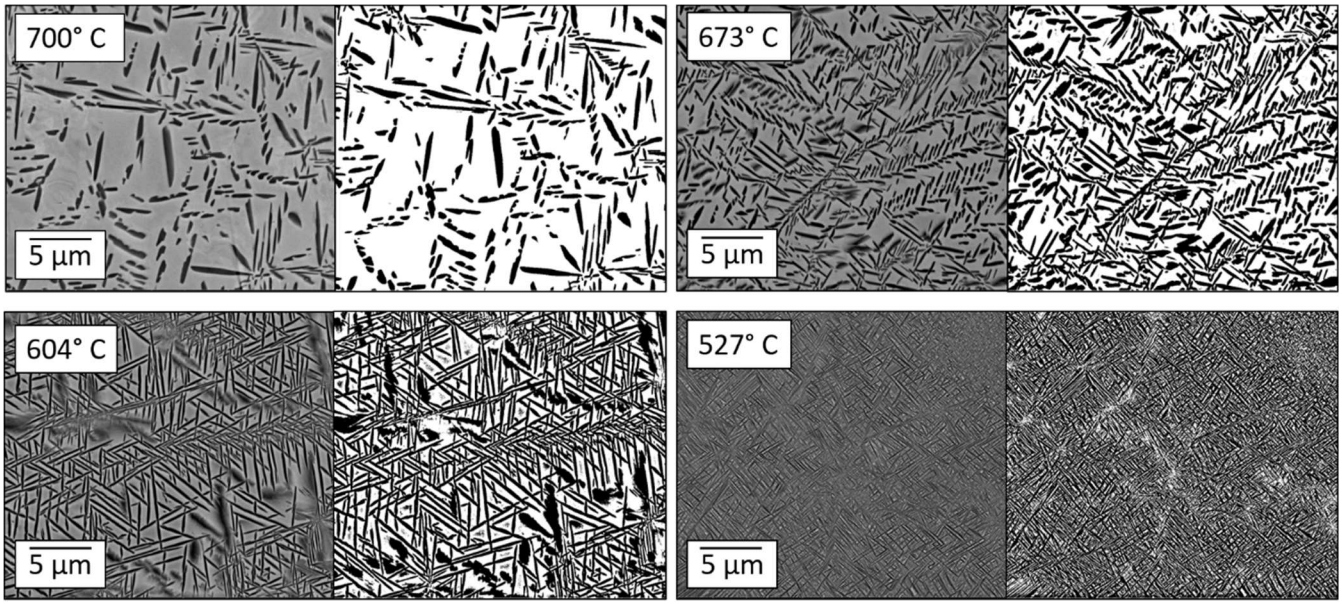

Figure 0.3- SEM backscatter images at the points of interest in the 4 hour thermally graded β-21S, next to the MIPAR images post processed to calculate the phase fractions. The changes in microstructure seen as the aging temperature changes is expected for these metastable β titanium alloys.

While there is the potential for much more characterization work on this sample, including the examination of the prior beta grain size and the regions between these four locations, the characterization work presented here is enough to demonstrate the viability of this procedure.

Conclusion

This method represents the next step in combinatorial materials science. Through the use of the Gleeble, and a carefully designed geometry, it has been shown that a gradient of temperatures can be induced in a single metal sample. Simulation techniques, such as COMSOL, can be used to guide the design of the geometry for the desired temperature gradient. β-21S was an ideal candidate to demonstrate this technique, owing to its sensitivity to aging temperature and the effect this has on the mechanical properties. While this method was verified with microstructural characterization and microhardness, this entirely new technique clearly has broad impact to materials process research. The ability to construct and hold a thermal gradient across such a small specimen further shows the usefulness and increasing viability of combinatorial metallurgy.

The authors gratefully acknowledge the support of the Center for Advanced Non-Ferrous Structural Alloys (CANFSA), a National Science Foundation Industry/University Cooperative Research Center (grant # 1624748), material provided by Timet, support under the Al and Julie Renken Professorship at Iowa State University, and the Materials and Analysis Research Laboratory (MARL) at Iowa State University.

CHAPTER 5. BICOMBINATORIAL METHOD APPLIED TO BINARY Ti-Cr SYSTEM

With the development of the thermal gradient method, the next step was to couple it with the existing methods of combinatorial approaches of LENS^{TM} composition gradients. This was done with a sample of Ti-(0-15)Cr wt%, in the shape appropriate to apply the thermal gradient Figure 0.1 – Schematic of the bicombinatorial experimental methods. This was characterized with optical and electron microscopy, showing variation in both composition and ageing temperature space, as well as quantification of average grain size changes and changes in microhardness. The methods demonstrated are a new path to rapid alloy exploration, screening, and optimization, where microstructural evaluation and trends can be tracked across composition changes and thermal treatment changes simultaneously.

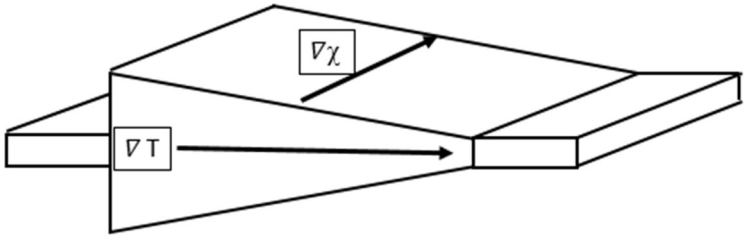

Figure 0.1 – Schematic of the bicombinatorial experimental methods

Results

Thermal gradient results and observations

Prior to the solutionization and ageing treatment of the full specimen, a smaller specimen was made to confirm that the changes in chemistry were not adversely affecting the homogeneity of temperature along the composition gradient. Changes in alloy chemistry affect physical properties, such as resistivity, and the concern was that these would lead to temperature gradients

in more than one dimension. The four thermocouples were attached to the four corners of this small specimen, and when brought to temperature no appreciable difference in temperature across the composition gradient was observed.

Figure 0.2 shows the temperature readout from the Ti-Cr gradient sample. An overall range from 500°C - 625°C was achieved. However, the range achieved with the β-21S was greater, and had a more linear profile across the entire length of the sample. Thus, in the Ti-xCr specimen, the full length was not used and there was a repetition of thermal histories. This could be due to the fact that the 21S was 1.5 inches thick, while the the Ti-xCr LENS^{TM} build was stopped when the full gradient was printed, and only reached 1 inch thick after machining. Not only did this result in less electrical contact with the Gleeble hot grips, resulting in slower heating response, the overall power input to the sample was 30% less. However, the stainless grips were the same size each time, and provided the same amount of a heat sink to both samples, with the Ti-xCr sample heated less. Moving forward with this technique, a wider sample will be preferred, with as much contact with the hot grips as possible.

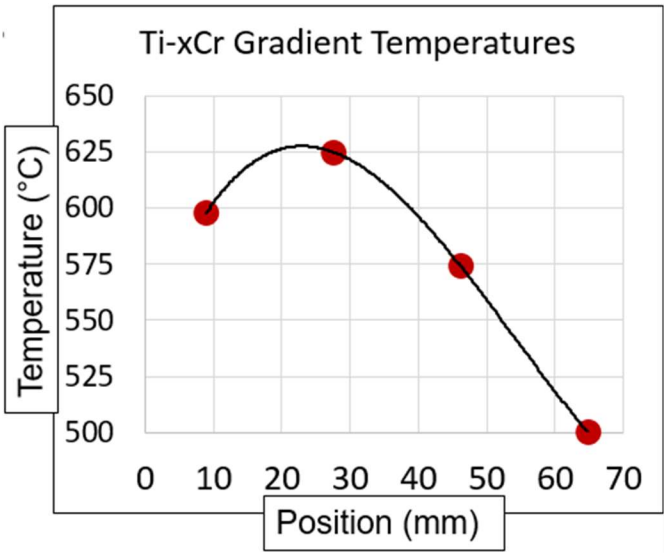

Figure 0.2 – Thermal profile of Ti-Cr bicombinatorial specimen.

Optical characterization

Figure 0.3 shows optical mosaics of the bicombinatorial specimen. There is a microstructural transition with respect to increasing Cr content. The changes are in both the size of the prior beta grains, and in the morphology of the underlying microstructure. In the areas of low (0-1 wt%) Cr, the microstructure is characteristic of CP titanium, with large, colony α laths and no β phase visible. Moving into the mid level of Cr concentration (2-8 wt%), the β grains that formed in the solutionization field, referred to as prior β grains, determine the morphology of the resulting α laths. Although not visible in the optical imaging, increasing Cr results in higher concentrations of retained β resulting in thicker β ribs, and smaller α laths. There is also a trend in increasing size of β grains in both increasing Cr concentration and increasing temperature. Finally, there is a sharp refinement of the microstructure in the higher (12-15 wt%) Cr. This is due to precipitation of $TiCr_2$, which forms preferentially on the grain boundaries, serving to pin said grain boundaries and impede grain growth. However, it would be expected that grain growth would take place not in the 500-625° C range, but upward of 1000° in the regime that the sample was β solutionized. While, as stated previously, the exact thermal profile is not known due to limitations on the thermocouples used, it can be assumed that the regions aged at 625° C experienced temperatures upwards of 1100° C during the 25 minute solutionization. The grain growth impedence high in the β phase field for the high Cr concentration regions indicates the formation of $TiCr_2$ during the printing. This phase only solutionizes above 1365° C and was thus retained during the solutionization treatments. Even bove the 1365° C martk, it has been reported to require longer solutionization times to dissolve [7,9].

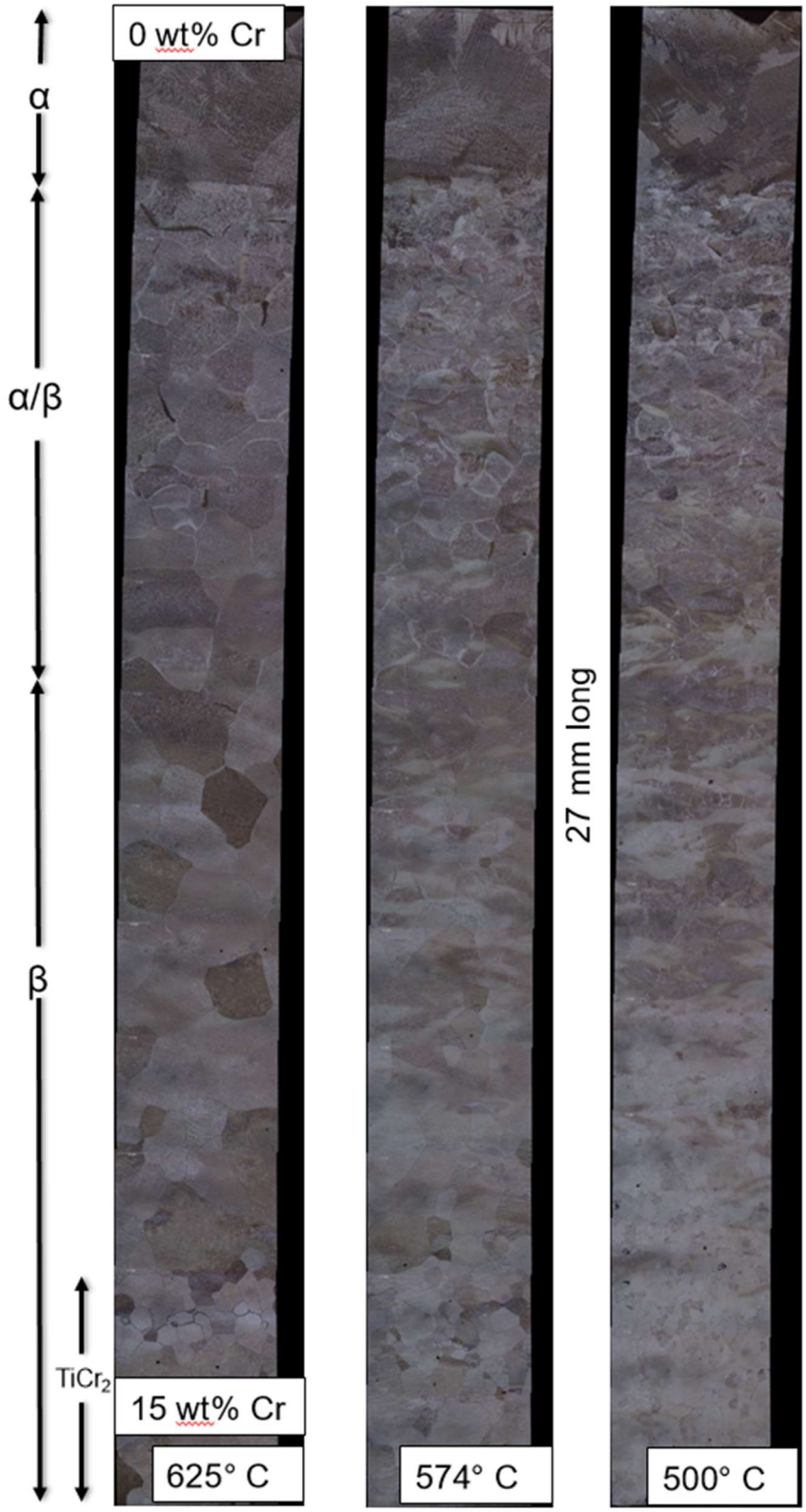

Figure 0.3 – Optical mosaic of Ti-Cr bicombinatorial specimen, with microstructure and alloy classification labeled.

The β grain size was also characterized quantitatively with respect to the thermal gradient. Regions of approximately the same composition were mapped for changes in grain size along the temperature gradient, and quantified using stereological methods developed for this purpose [49]. As mentioned previously, due to the lack of thermal monitoring in the solutionization regime it is impossible to know what the thermal profile was like during the periods of grain growth. However, quantification of the prior β grain size puts a clear trend on the effect of the gradient thermal treatment on the resulting microstructure, with a steady increase in size following the thermal profile closely. Quantification provides more insight to the compositional effects, where prior β grain size is relatively constant with respect to composition in the 4-8% Cr regions, and drastically drops in seize with the onset of $TiCr_2$ precipitation.

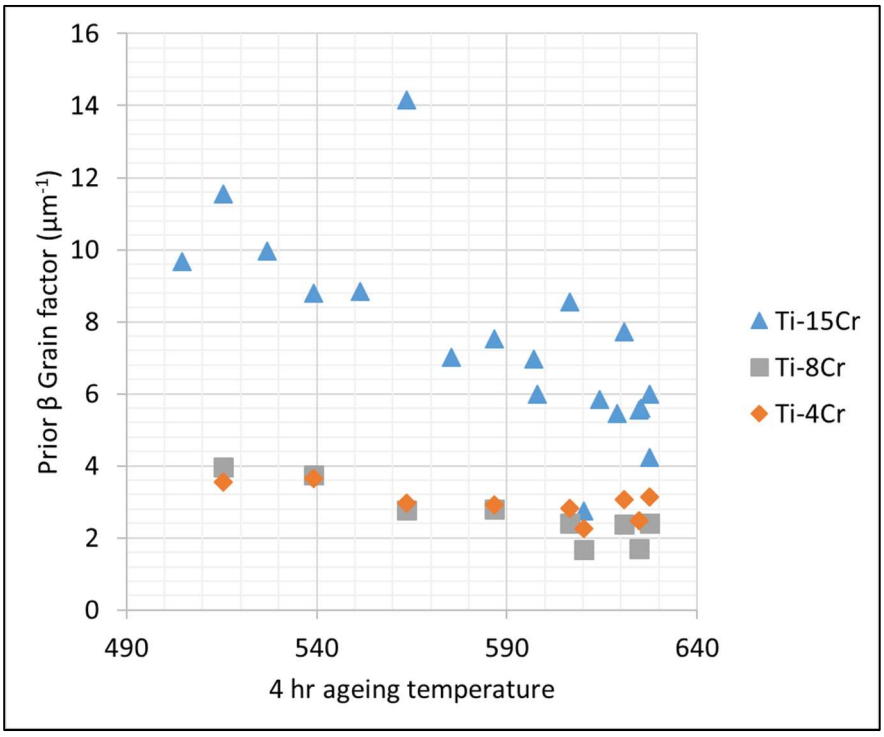

Figure 0.4 – Prior beta grain factor, plotted against the ageing temperature

SEM imaging

The sample was characterized with SEM using both backscatter electrons, and electron dispersal spectroscopy (EDS) to verify the bulk composition within the specimen. Figure 0.5 shows some SEM images along both the composition gradient and thermal ageing temperature gradient. The low compositions of Cr result in the typical Wiedmanstaaten α laths, where the *hcp* α structure is formed at almost complete exclusions of the *bcc* β. The structure is also almost entirely colony. Moving into the mid-level rage of Cr, the effects of the thermal gradient on the microstructure becomes more evident. Coarsening of the laths as a result of higher ageing temperature is apparent, and the α/β microstructure transitions to a basketweave structure, with interlocking laths in many different orientations. As Cr is a β stabilizer, increasing Cr concentration results in a higher concentration of β and thicker β ribs, and thinner α laths. The transition from the α/β microstructure into the metastable β is seen in the 7-9 wt% region. Here, it would be equally valid to describe this region as a β matrix, with suspended α platelets, as it would to say it is a network of α laths with β in between. Since this specimen was not quenched after β solutionization, but rather brought down from the solutionizing temperature directly to the ageing temperature, there was no opportunity for the formation of the martensitic α' phase, retention of which is the distinction between α/β alloys and β alloys. Also of note, the effect of different ageing temperatures becomes more dramatic, especially in the 500° C regime.

Figure 0.6 shows further SEM images, across the single composition of 15 wt% Cr. Here, the sluggish precipitation of the $TiCr_2$ Laves phase [9,10,27] highlights the usefulness of the thermal gradient treatment. Subtle changes in the ageing temperature, and thus the amount of undercooling effecting phase transitions from β to α + $TiCr_2$, show a progression of the formation of the Laves phase. In the lower temperature region shown, which is also

representative of temperatures lower than 570° C, the bright dots of this phase are scattered sparsely throughout the bulk of the grains, and occasionally grouping up on the grain boundaries. Moving to higher temperature regions shows a larger amount of growth at the grain boundaries, and finally to the highest temperatures observed has the Laves phases growing in clusters with the α phase both along grain boundaries, and in the bulk of the grains.

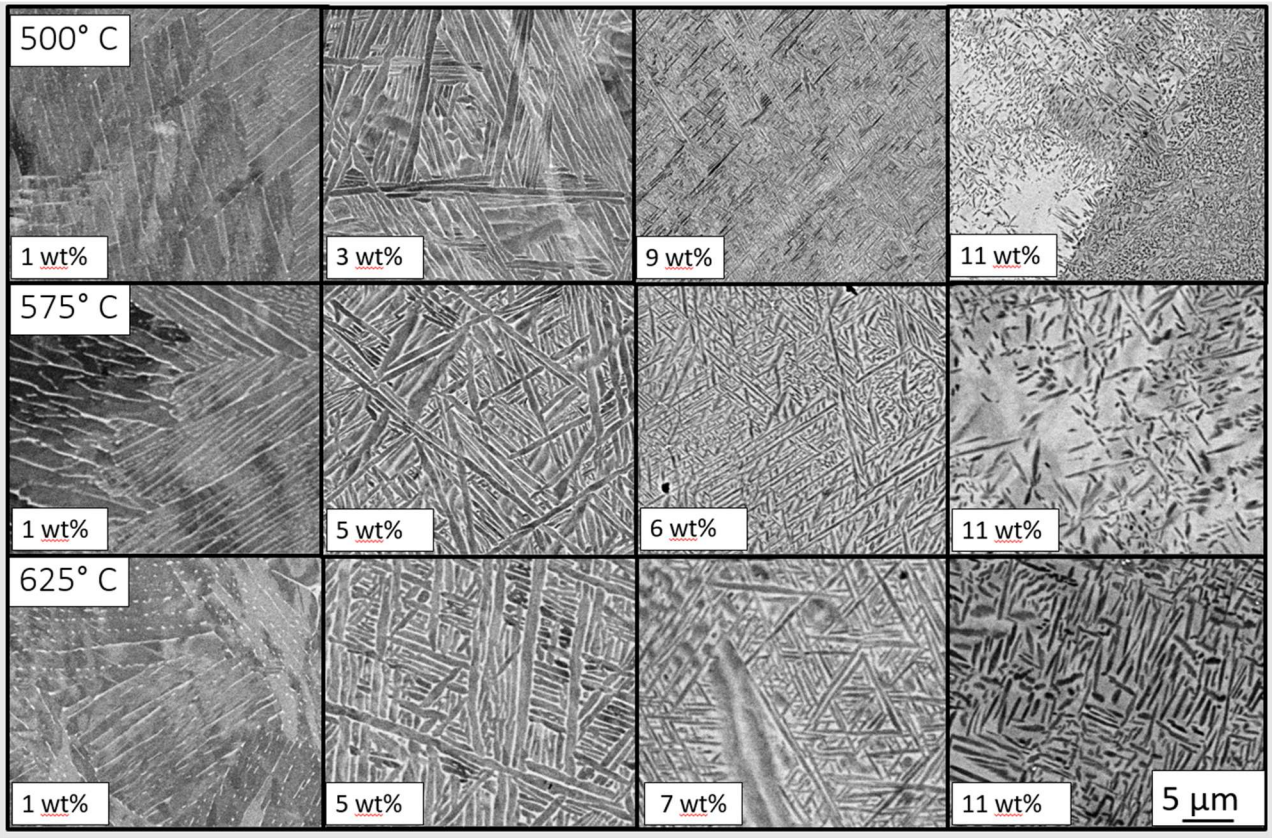

Figure 0.5 – SEM backscatter images of the Ti-Cr bicombinatorial specimen.

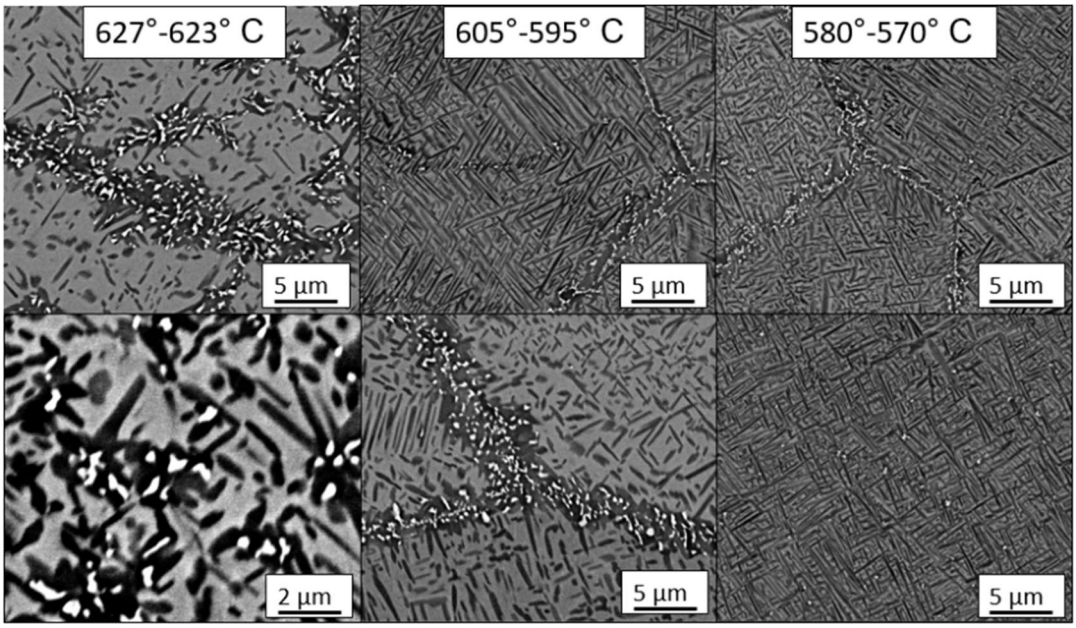

Figure 0.6 – Ti-15Cr wt% region, showing effect on ageing temperature on the morphology of the $TiCr_2$ Laves phase

Microhardness testing

Hardness testing was performed on the bicombinatorial sample. Each point on the graph in Figure 0.7 represents an average of four indents taken at a point in a grid. Predictably, the greatest trend is an increase in hardness with increasing Cr concentration, due to the solid solution strengthening offered by the substitutional Cr atoms. However, this increase in hardness due to increasing Cr content begins to depreciate around the 7 wt% Cr mark, especially in the regions subject to higher ageing temperature. Higher ageing temperatures leads to decreased hardness values for compositions above ~7 wt%. These areas correspond to the metastable β type microstructure, where the morphology of the precipitated α laths is the major determinate of strength. Again, as seen with the β-21S, the lower ageing temperatures leads to a finer scale α structure, and thus an increased hardness. The lower Cr concentration had large fluctuations in hardness value, with no clear trend. Since these regions are largely α phase, the solid solution

strengthening would be much less pronounced, due to the low solubility of Cr in α. As seen in Figure 0.5, there was little microstructural variation across the thermal gradient in these regions.

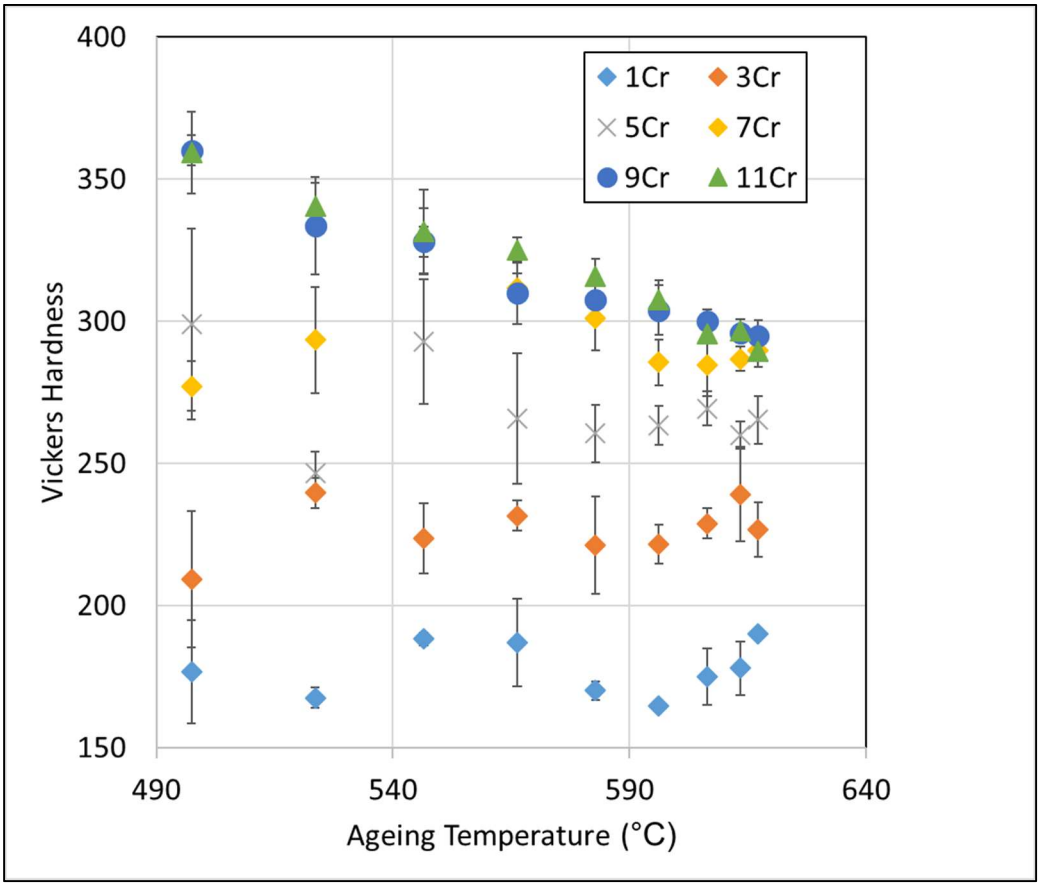

Figure 0.7 – Microhardness values for Ti-Cr specimen.

Conclusions and Future Work

- Existing methods of combinatorial materials science using composition gradients generated with the LENS^{TM} have been successfully coupled with a newly developed technique of applying thermal gradients, which take advantage of the resistive heating capabilities of the Gleeble thermomechanical simulator. This has been applied to a Ti-(0-15) Cr sample, with a thermal gradient of 500-625° C.

- The Ti-Cr specimen has been characterized with optical and electron microscopy, as well as with microhardness, to demonstrate gradients in structure and properties. Prior β grain size, α lath morphology, and microhardness values have been tracked in both temperature and composition space, connecting processing, microstructure, and properties both quantitatively and qualitatively.
- This technique represents the next step forward in combinatorial materials science. Rapid alloy screening can be done on new alloy systems demanding investigation, as well as existing systems that have not been revisited in over 30 years. These new tools and techniques can also be applied to basic science studies in the realms of thermodynamics, phase stability, phase transitions and growth, grain growth and diffusion. Like never before, the potential to perform multiple experiments in a single sample allows for an greater degree of freedom in decisions regarding the next steps to take in metallurgy.

CHAPTER 6. APPLICATION OF BICOMBINATORIAL METHOD TO DEVELOPMENT OF NEW OXIDATION AND CREEP RESISTANT TITANIUM ALLOY

With the methods of developing and utilizing this new bicombinatorial method, the application of this technique to a new multicomponent alloy system is the next step. The creep resistance of β-21S has long been a limiting factor in its use, and the improvement of creep properties, while maintaining oxidation resistance and cold rollability, would be a major step. Replacing Mo in 21S with Cr could result in favorable mechanical properties. Oxidation tests in the manner developed by Samimi [12,32,33] provided the first step to select the Cr concentration, and application of the bicombinatorial method to screen for Si content was followed by drop casting of large rods for creep tests in the Gleeble.

Development of Titanium β-21S: β Alloy for High Temperature Oxidation Resistance

β-21S, as the name suggests, is a metastable β titanium alloy of composition Ti-15Mo-3Al-2.7Nb-0.2Si wt% that has found use in the aerospace industry. This is primarily due the cold rollability and age hardenability inherent to all β alloys, combined with oxidation and corrosion resistance unique to this alloy. The development of this particular alloy, by Bania and Parris working for Timet around 1990 [50], was motivated to fulfil a specific purpose: replacing Ti-15-3 (Ti-15V-3Cr-3Sn-3Al) in metal matrix composites used in airframe manufacturing [51]. Poor high temperature oxidation performance of Ti-15-3 became a limiting factor for their customers. It was desired to develop a new β titanium alloy, maintaining the cold rollability and age hardinability of Ti-15-3, but that could provide improved oxidation resistance. In this effort, Bania and Parris focused on Mo and Cr as the primary alloying elements. Various compositions based on these were button melted, and screened with a 50% reduction cold rolling. If there was

no cracking, the coupons were subjected to high temperature oxidation testing, the results of which are show in Figure 0.1.

From these tests, Mo was selected as the primary alloying element, with Nb and Si selected as secondary additions due to reducing the oxygen weight gain the most. Additional oxidation tests were performed to determine the smallest additions of Nb and Si that would continue to provide the excellent oxidation resistance, and Al was added to improve the mechanical properties, due to it stabilizing the α phase. This resulted in a β alloy that has high temperature oxidation resistance better than CP titanium and Ti-15-3 [51], while still maintaining the cold rollability of β alloys [5]. The alloy has also found use due to its resistance to hot hydraulic fluid, which in most other titanium alloys will etch and fill with hydrogen, severely embrittling the material [5,52]. This has allowed it to be used in areas of jet engines traditionally off limits to titanium alloys, resulting in 74 kilograms of weight reduction for the Boeing 777 [5].

Initial Oxidation Results: 48 Hr/1500°F Exposure

(250 gm Button Heats: .060" Cold Rolled Coupons)

Alloy	% Wt. Gain	Alloy	% Wt. Gain
Ti-15V-3Cr-3Sn-3Al	All Oxide, >65	Ti-15Cr-.2Pd	9.76
Commercially Pure (Gr. 2)	7.70	Ti-15Cr-3Ta	9.44
Ti-15Mo-5Zr	7.70	Ti-15Cr-5Nb	7.62
Ti-15Mo-3Sn	5.37	Ti-15Cr-.5Si	7.00
Ti-15Mo-5Co	2.89	Ti-15Cr-3Sn	4.11
Ti-15Mo-.1Y	2.73	Ti-15Cr-3Al	3.68
Ti-15Mo-5Re	2.68	Ti-15Cr-5Mo	2.90
Ti-15Mo	2.63	Ti-15Cr	2.27
Ti-15Mo-5Fe	2.10		
Ti-15Mo-3Al	2.00		
Ti-15Mo-.2Pd	1.79		
Ti-15Mo-.1Si	1.45		
Ti-15Mo-5Hf	1.41		
Ti-15Mo-.2Si	1.27		
Ti-15Mo-.5Si	1.17		
Ti-15Mo-3Ta	1.04		
Ti-20Mo-2Nb	.99		
Ti-15Mo-2Nb	.98		
Ti-15Mo-5Nb	.95		

Figure 0.1 – Results from oxidation tests done in development of β-21S [50]

Investigation of New Titanium Alloy Systems

Despite the attractive properties of β-21S, related to the relative ease of production and chemical resistance, there is still a gap in the mechanical properties between β alloys in general and alloys formed primarily of α. While β-21S is remarkable in being able to match the creep resistance of Ti-6Al-4V, it still does not come close to α or near α alloys such as Ti-6242 [51]. This increase in strength is largely due to the nature of the different crystal structures. The hcp system has far fewer slip systems than the bcc, making dislocation motion more difficult, and a higher strength. In creep properties of these β alloys, discussed earlier, the differences are even more pronounced. Considering that the refinement and control of the α precipitates in β titanium alloys can only provide so much strength, exploring new alloy composition space must be considered. Precipitation of intermetallic compounds in the β matrix alongside α could greatly enhance the creep properties of these β alloys.

The selection of Cr for its potential to strengthen the β titanium alloy relied on several factors. Cr is one of the most common β stabilizers after V and Mo, and the eutectoid formation of the $TiCr_2$ has already been discussed here, in both the literature and the observations made in the Ti-Cr bicombinatorial demonstration. Additionally, Cr was considered as the primary alloying element in the development of β-21S, but did not exhibit the desired oxidation resistance required by Bania and Parris. However, with the addition of the work done by Samimi on the nature of the oxidation resistance of Cr in Ti [12], this system demands a second look. Oxidation resistance of 21S is usually attributed to the slow diffusion of Mo, combined with synergistic effects from Al, Nb and Si. The replacement of Mo with Cr in 21S could preserve the oxidation properties while improving creep.

Oxidation tests of new alloy system

The first step in this was to confirm the oxidation resistance of this proposed new alloy, and see if the same critical concentration of Cr behavior found by Samimi could be replicated. The same steps were taken to perform a combinatorial oxidation study, using the LENS^{TM}, and varying composition of Cr. The range of Cr concentration would hopefully capture the same pattern. Since Samimi saw the critical Cr concentration at 20 wt%, it was decided to go up to 25 wt% Cr. The lower end was determined by preserving the Mo equivalency of 21S. By the Mo equivalency equation, 15 wt% Mo is equivalent to 12 wt% Cr. The lower bound of Cr was then set to 10 wt% Cr. The elemental powder blends used are shown in Table 0.1.

Table 0.1 – Powder weight percentages used for oxidation study gradient, compared to EDS of deposition.

	Ti	Cr	Al	Nb	Si
wt% A Powder	Balance	10	3	2.7	0.2
wt% B Powder	Balance	25	3	2.7	0.2
EDS of A	Balance	5	2.5	1.5	0.2
EDS of B	Balance	20	2.5	1.5	0.2

Figure 0.2 shows the results of the oxide scale measurements. These by measuring the oxide scale thickness at four independent locations for each composition using the SEM, with composition verified using EDS. Four independent measurements were done at each composition level and averaged. The same critical Cr content found in the binary Ti-Cr system is observed for the multicomponent system here. The addition of Al, Nb and Si lower the concentration to only 10 wt%. SEM analysis of the microstructure (Figure 0.3) shows that the formation of the Laves

phase is occurring at lower concentrations of Cr. It is possible that the presence of Al serves to accelerate this through a solute rejection process. Al serves to stabilize the α phase, which ejects Cr and enriches the surrounding β with Cr, as the solubility of Cr in α Ti is 0.47 at.% at 667° C [6]. This enrichment of the surrounding β phase induces the formation of the Laves phase. Oxygen (O), an even stronger α stabilizer, would further increase the fraction of α and accelerate the formation of the Laves phase, leading to the fine scale Laves phase on the surface that inhibits oxygen ingress and oxide growth. This is the same microstructural development observed by Samimi in the investigation of the oxidation behavior of binary Ti-Cr [12]. In the 20% Cr region, the structure even looks closer to cooperative growth, with the Laves phase appearing in a lamellar like fashion alongside the α.

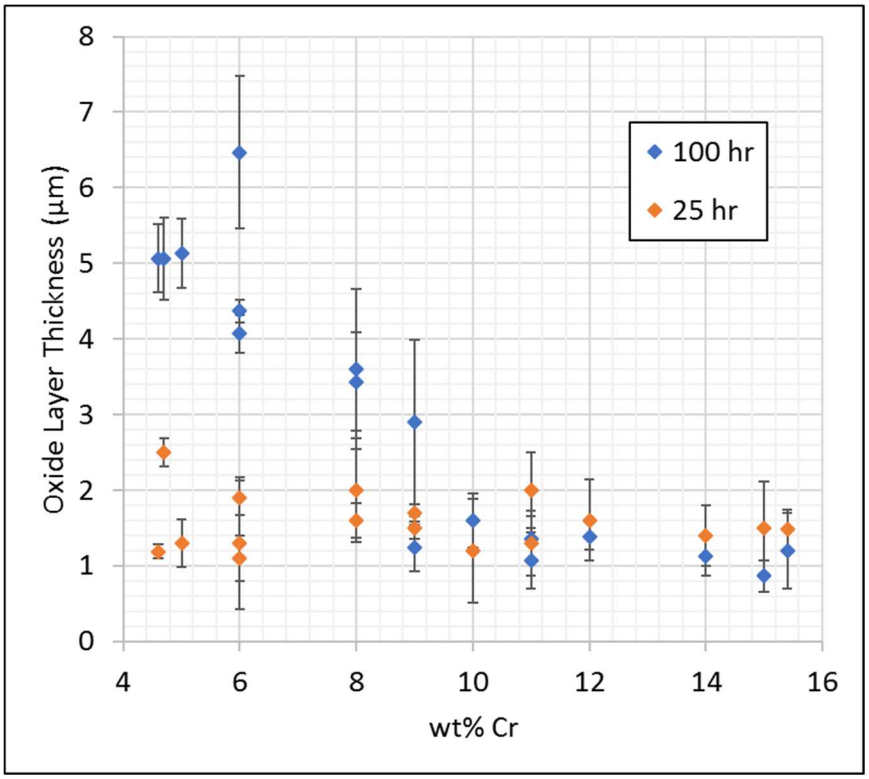

Figure 0.2 – Results from oxidation studies of Ti-xCr-3Al-2.7Nb-0.2Si, oxidized at 650° C. Error bars represent standard deviation of the four independent measurements taken for each composition

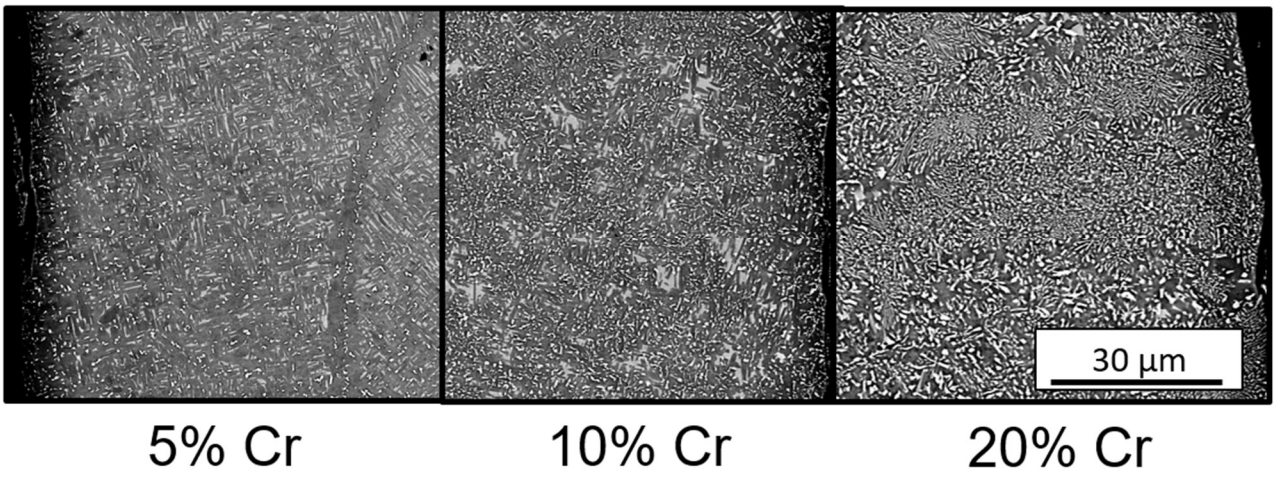

Figure 0.3 –Microstructural changes for gradient Ti-(5-25)Cr-3Al-2.7Nb-0.2Si

Application of the Bicombinatorial Approach

With the percentage of Cr determined, the next step was to examine microstructural changes as a result of increased Nb and Si content. Nb and Si are both known to increase creep resistance of Ti, provided there are no other detrimental microstructural changes. In the case of Si, the solid solution strengthening provides the best use of Si; silicide formation could be detrimental, as shown by Winstone et al [26]. Any excessive silicide formation would not only serve to embrittle the structure, but these tend to cluster on grain boundaries, leading to rapid void formation, followed by crack nucleation and failure. If brittle failure or rapid crack nucleation is observed, it would not be certain whether that was due to the $TiCr_2$ based system, or the additional presence of silicides. At this stage in alloy development, any silicon-rich particles would be undesirable. The same effects on silicide formation would also be monitored with increasing Nb content, as well as any other possible unknown effects.

Investigation of this system utilized the newly developed bicombinatorial approach. As described in Chapter 3, using 3 different powder blends both Si and Nb content was varied in a single build, in the shape required to apply the Gleeble thermal gradient technique. The thermal

profile recorded from the four thermocouple readouts is given in Figure 0.4. After the results of the binary Ti-Cr bicombinatorial thermal gradient, extra effort was made to ensure the build was as tall as possible, and the resulting thermal profile shows a much wider range of temperatures as a result.

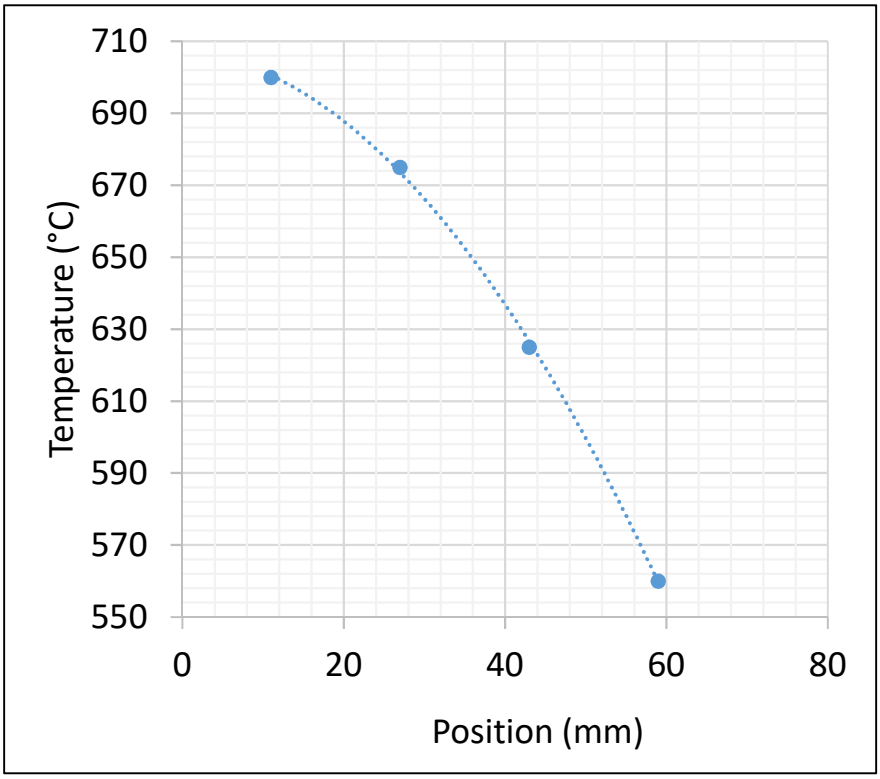

Figure 0.4- Thermal profile from thermocouple readouts on the $TiCr_2$ based bicombinatorial study.

Results

Despite efforts to mitigate its effects, the presence of Nb prevented complete melting or mixing of the samples, and the composition of Nb in the microstructure across the entire sample remained ~0.8 wt%. However, characterization of the Si gradient, as well as the effects of the thermal gradient, was still possible. Firstly, the presence of Si-rich precipitates was investigated. Figure 0.5 shows SEM images across various bulk compositions of Si. Even with small increases

in Si concentration, a much darker phase is seen close to the α-$TiCr_2$ formations. Increasing concentration up to 0.6 wt% shows the formation of this phase more clearly, with 1 wt% Si resulting in Si-rich substructures. Only in the regions where the Si concentration is kept the same as is found in β-21S is there a lack of this fourth phase. EDS analysis confirmed these dark phases to be Si-rich, indicating the formation of silicides. As stated previously, any amount of silicide formation is undesired, so the final composition was kept at 0.2 wt% Si. Nb, which was unable to be studies, was kept at the 3 wt% found in β-21S and used in the oxidation studies.

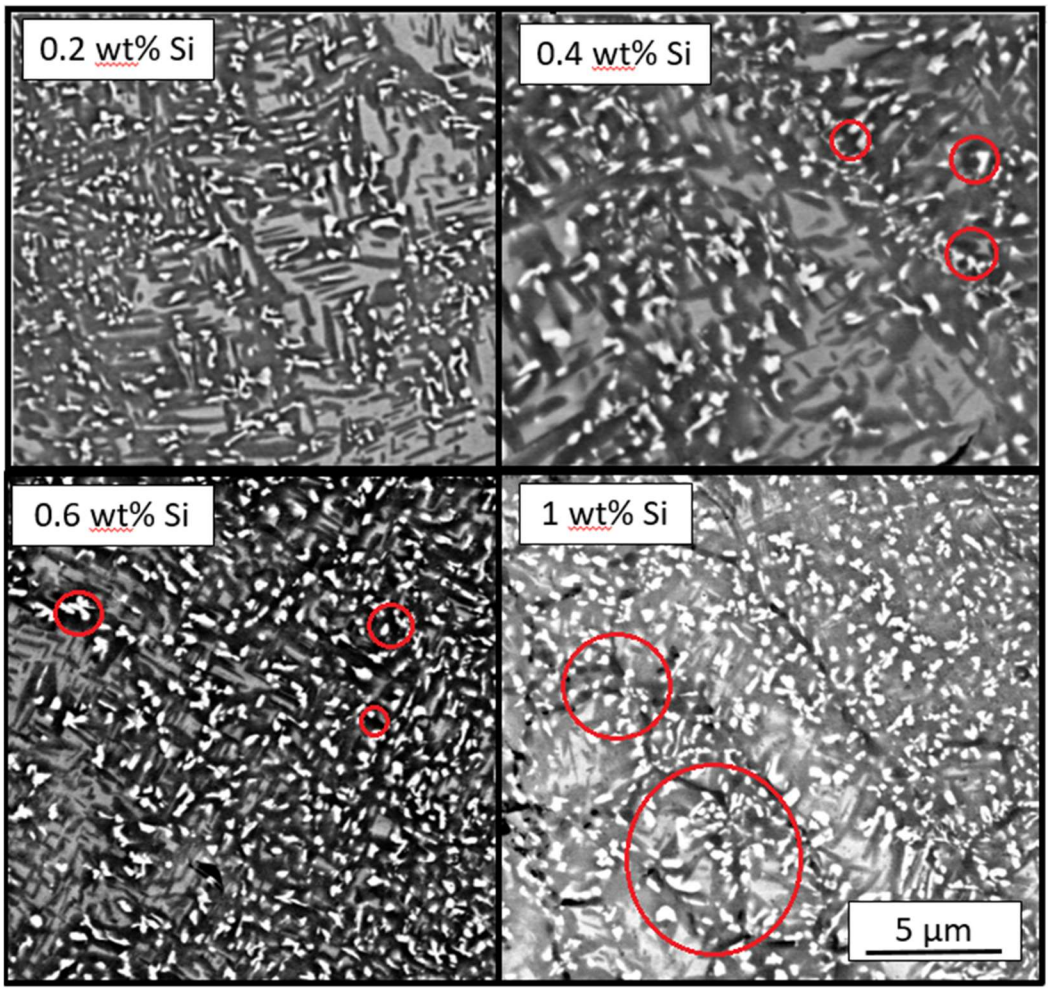

Figure 0.5 – SEM images showing formation of Si rich particles across a range of Si content. Features in question are circles in red, and found forming next to the bright Cr-rich Laves phases

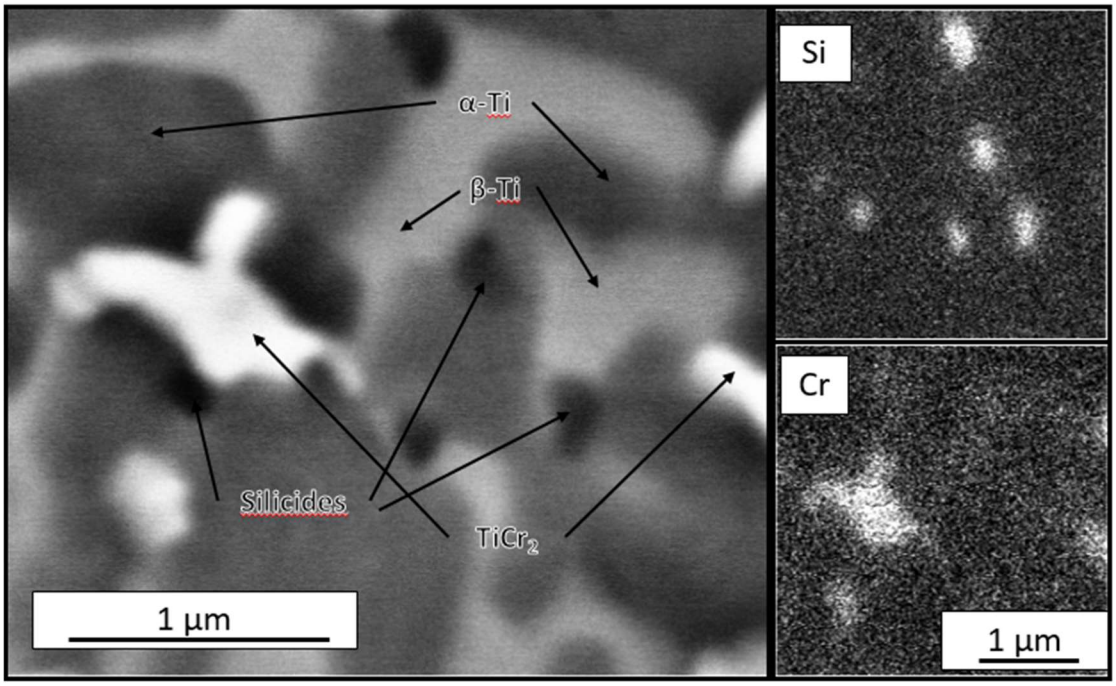

Figure 0.6 - EDS map of Ti-10Cr-2Al-0.5Nb-0.6Si, showing Si-rich particles along the α boundaries, as well as maps of signal for Si and Nb

The thermal gradient effects were also studied. As expected, the lower ageing temperatures resulted in a much finer microstructure. However, in the case of many Ti alloys designed for high temperature use, a higher ageing temperature lends itself to greater thermal stability of the microstructure as a whole, due to development of an overaged microstructure. Even if a finer distribution of α laths lead to improved mechanical properties through inhibition of dislocation motion, they may not remain stable. However, as state previously, the $TiCr_2$ phase is highly thermally stable, and only goes back into bcc solution above 1365° C. Figure 0.7 shows the effect on microstructure of this new alloy as a result of the different ageing temperatures. The lower temperature ageing regime results in a much finer scale microstructure, which increases strength and creep resistance of β-Ti alloys [20,21,53].

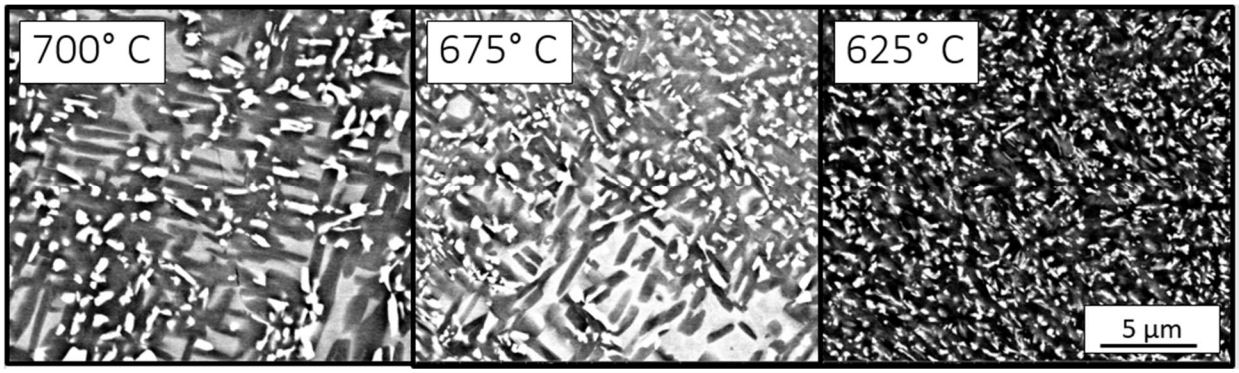

Figure 0.7 – Ti-10Cr-3Al-0.8Nb-0.2Si aged at different temperatures

Creep Tests of New Alloy Composition

Validation of Gleeble creep testing

Before study of the creep behavior of the new alloy could be done, baseline tests of β-21S were carried out. Two ageing regimes were performed on the β solutionized samples: 700° C for 8 hrs, and 593° C for 8 hours. The 700° C ageing was done to replicate the work done by Peterson [20] in the studies of creep in 21S. The same stress and temperature regimes were used, to further ensure that the Gleeble could be used to reliably produce creep test results.

Selection of alloy composition

The composition Ti-10Cr-3Al-3Nb-0.2Si wt% was selected for final creep testing, with drop casting done as described in Chapter 3. This was solutionized at 1000° C for 30 minutes, water quenched while still encapsulated, and taken to the ageing temperature of 600° C for 8 hours, from results of the thermal gradient tests.

Results

Table 0.2 shows results from the creep tests done in the Gleeble, with previous results from Peterson using the ETMT shown. Figure 0.8 is Larson-Miller plot with these results [20]. In

terms of validating the methods developed for the Gleeble in performing creep tests, the results here align well with previous studies using thermomechanical simulators. The current flow affecting creep rate is carried over, even though the ETMT is a DC current, but the Gleeble is AC. In this case, the hypothesis of electron wind being a factor fails. Here, since the dominant creep method is not mass diffusion but dislocation flow, so it is better to think of the electric field effects as a lowering of dislocation activation energy than a "wind" effect. Regardless of the exact causes, the studies still confirm the Gleeble as a potential tool for creep testing.

Table 0.2 – Results from creep tests performed on Gleeble, compared to previous work done on ETMT [20]

	Stress (MPa)	**T (°C)**	**$t_{0.2\%}$**	**$P = T(20+\log(t_{0.2\%})/1000)$**
21S - ETMT	400	400	108000	14.54
	200	450	30600	15.13
	50	650	216	17.33
21S - Gleeble, 700	400	400	155000	14.56
	200	450	38050	15.20
	50	650	400	17.58
21S - Gleeble, 593	200	450	108000	15.53
	50	650	200	17.30
Laves Alloy	400	400	2000	13.29
	200	450	600	13.90
	50	650	50	16.75

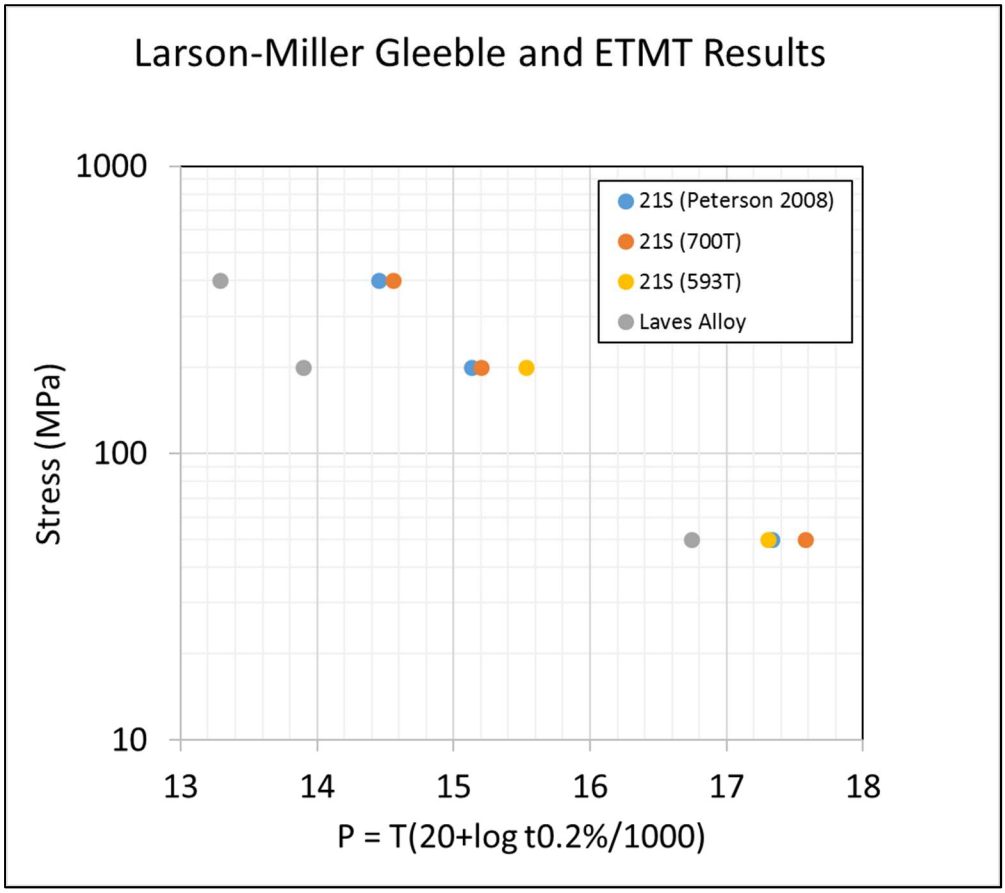

Figure 0.8 – Larson-Miller plot of β-21S, aged, and newly developed Laves Alloy.

The testing of the two different ageing treatments of β-21S is also shown. Here, the lower ageing temperature resulted in finer scale α and a better creep performance in the 450° C samples. In the 650° C tests, which can be considered accelerated creep tests, the 593° C aged samples had noticeably poorer performance. This is most likely due to slight variations in testing conditions having higher effect in the shorter test times. This is also a higher testing temperature than the sample was aged at, meaning there could still be growth of the α laths leading to a mechanical response. For the highest stress regime of the 593° C test, anomalous behavior prevented good comparisons from being made.

The creep performance of the Laves alloy is noticeable poorer than the performance of the β-21S. These results are surprising, considering the general high strength of the Laves phases at elevated temperatures. This could suggest that solid solution strengthening has a much higher contribution that previously considered. In the case of 21S, the primary alloying element, Mo, remains entirely in solution in the bcc lattice, where the Cr in the Laves alloy is mostly concentrated in the Laves precipitates. The oxidation performance of the alloy is still good, and additional study could lead to this being a viable new system, especially considering the lack of serious studies on the potential for Laves phase strengthened titanium alloys.

Conclusions and Future Work

- The bicombinatorial technique has been applied to a new titanium alloy system, using the $TiCr_2$ Laves phase as the primary strengthening mechanism. Though it, this previously unexplored alloy system was verified for oxidation resistance and studied for effects of variations in silicon content using composition gradients generated with the LENS^{TM}. Using the thermal gradient method, the effect of different ageing temperatures on the final microstructure was studied. This method has thus been demonstrated as a powerful new tool for rapid alloy exploration in both composition and temperature space.
- Techniques have been developed to use the Gleeble as a creep testing mechanism. These tests were run on β-21S, to compare with previous work done on the ETMT. While these machines can provide fine-tuned thermal control through the use of direct resistive heating, this heating method also leads to increased creep rates through presently unknown mechanisms. While effects from dislocation activation energy reduction, or electron wind have been hypothesized, the exact effect of the applied current on mechanical properties demands further study.

- The new alloy composition of Ti-10Cr-3Al-3Nb-0.2Si has been creep tested in the Gleeble. While the performance was poorer than other titanium alloys, the oxidation performance and high temperature mechanical properties of the Laves phases mean that this study could be used as a starting point for further exploration of this system.

REFERENCES

[1] G. Lütjering, J. Williams, Titanium, Springer Berlin Heidelberg, Berlin, Heidelberg, 2003.

[2] H.W. Rosenberg, The Science, Technology and Application of Titanium, Pergamon Press, Oxford, UK, 1970.

[3] E.K. Molchanova, (1965).

[4] R. Boyer, G. Welshc, E.W. Collings, Materials Properties Handbook: Titanium Alloys, ASM, Materials Park, USA, 1994.

[5] R.R. Boyer, Mater. Sci. Eng. A 213 (1996) 103–114.

[6] J.L. Murray, Bull. Alloy Phase Diagrams 2 (1981) 174–181.

[7] D.M. Cupid, M.J. Kriegel, O. Fabrichnaya, F. Ebrahimi, H.J. Seifert, Intermetallics 19 (2011) 1222–1235.

[8] R.H. Ericksen, R. Taggart, D.H. Polonis, Acta Metall. 17 (1969) 553–564.

[9] K.C. Chen, S.M. Allen, J.D. Livingston, J. Mater. Res. (1996).

[10] K.C. Chen, S.M. Allen, J.D. Livingston, Mater. Sci. Eng. A 242 (1998) 162–173.

[11] J.D. Livingston, Phys. Status Solidi. A. 131 (1992) 415–423.

[12] P. Samimi, Y. Liu, I. Ghamarian, D.A. Brice, P.C. Collins, Corros. Sci. 97 (2015) 150–160.

[13] D.J. Thoma, J.H. Perepezko, J. Alloys Compd. 224 (1995) 330–341.

[14] F. Chu, T.E. Mitchell, S.P. Chen, 18 (1997) 536–543.

[15] M. Kassner, Fundamentals of Creep in Metals and Alloys, 2nd ed., Elsevier, 2008.

[16] R.W. Evans, B. Wilshire, Introduction to Creep, Institute of Materials, London, 1993.

[17] K.K. Chawla, Mechanical Behavior of Materials, Prentice Hall, Upper Sadle River, NJ, 2002.

[18] J. Hult, Creep in Engineering Structures, Blaisdel Publishing Company, Waltham, 1966.

[19] F.R. Larson, J. Miller, Trans. ASME 74 (1952) 765–771.

[20] B. Peterson, A Combinatorial Approach to the Development of a Creep Resistant Beta Titanium Alloy, The Ohio State University, 2008.

[21] L. Ponsonnet, C. Quesne, R. Penelle, Mater. Sci. Eng. A 262 (1999) 50–63.

[22] R.T. Chen, W.H. Miller, E.A. Starke, TMS Pap. Sel. 56 (1984).

[23] J. Koike, K. Maruyama, Mater. Sci. Eng. A 263 (1999) 155–159.

[24] S.L. Semiatin, T.R. Bieler, Acta Mater. 49 (2001) 3565–3573.

[25] W. Parris, P. Bania, US 4980127 A, 1991.

[26] M.R. Winstone, R. Rawlings, D.R.F. West, J. Less-Common Met. 39 (1975) 205–217.

[27] D. Northwood, I. Smith, J. Mater. Sci. Lett. 6 (1987) 820–822.

[28] T. Takeda, W.M. Steen, D.R.F. West, ICALEO ’84 44 (1984).

[29] W.M. Steen, R.M. Vilar, K.G. Watkins, M.G.S. Ferreira, P. Carvalho, C.L. Sexton, M. Pontinha, M. McMahon, ICALEO ’92 (1992) 278–287.

[30] K.I. Schwendner, R. Banerjee, P.C. Collins, C.A. Brice, H.L. Fraser, Scr. Mater. 45 (2001) 1123–1129.

[31] P.C. Collins, R. Banerjee, S. Banerjee, H.L. Fraser, 352 (2003) 118–128.

[32] P. Samimi, Y. Liu, I. Ghamarian, P.C. Collins, Corros. Sci. 89 (2014) 295–306.

[33] P. Samimi, Combinatorial Assessment of the Influence of Composition and Exposure

Time on the Oxidation Behavior and Concurrent Oxygen-Induced Phase Transformations of Binary Ti-X Systems, University of North Texas, 2015.

[34] M.Y. Mendoza, P. Samimi, D.A. Brice, B.W. Martin, M.R. Rolchigo, R. LeSar, P.C. Collins, Metall. Mater. Trans. A Phys. Metall. Mater. Sci. 48 (2017) 3594–3605.

[35] Dynamic Systems Incorporated, Gleeble Users Training, Poestenkill, 2015.

[36] S.A. Mantri, D. Choudhuri, A. Behera, J.D. Cotton, N. Kumar, R. Banerjee, Metall. Mater. Trans. A Phys. Metall. Mater. Sci. 46 (2015) 2803–2808.

[37] P. Samimi, Y. Liu, I. Ghamarian, P.C. Collins, Corros. Sci. 89 (2014) 295–306.

[38] R. Banerjee, S. Nag, H.L. Fraser, Mater. Sci. Eng. C 25 (2005) 282–289.

[39] ASTMA255, (2014).

[40] Y. Hanghang, Y. Zekun, G. Jun, G. Hongzhen, L. Yingying, W. Min, Rare Met. Mater. Eng. 39 (2010) 22–26.

[41] A. Tejfalussy, Temperature Distribution Regulating Sample Holder-Adapter for Forming Conditions for Gradient Heat Treatment in Heat Treatment Ovens or Furnaces, 4609343, 1986.

[42] J. Gayda, T. Gabb, P. Kantzo, Heat Treatment Devices and Method of Operation Thereof to Produce Dual Microstructure Superalloy Disks, US6660110 B1, 2003.

[43] G. Tian, C. Jia, J. Liu, B. Hu, Mater. Des. 30 (2009) 433–439.

[44] Y. Ning, Z. Yao, H. Guo, M.W. Fu, J. Alloys Compd. 557 (2013) 27–33.

[45] S.T. Mandziej, Mater. Tehnol. 44 (2010) 105–119.

[46] I. Weiss, S.L. Semiatin, Mater. Sci. Eng. A 243 (1998) 46–65.

[47] J.M. Sosa, D.E. Huber, B. Welk, H.L. Fraser, Integr. Mater. Manuf. Innov. 3 (2014) 10.

[48] S. Ankem, C.. Greene, Mater. Sci. Eng. A 263 (1999) 127–131.

[49] J. Tiley, T. Searles, E. Lee, S. Kar, R. Banerjee, J.C. Russ, H.L. Fraser, Mater. Sci. Eng. A 372 (2004) 191–198.

[50] P.J. Bania, W.M. Parris, in:, Titan. 1990 Prod. Appl. Proc. Tech. Progr. from 1990 Int. Conf., 1990, pp. 784–793.

[51] P.J. Bania, ISIJ Int. 31 (1991) 840–847.

[52] J.S. Grauman, Beta Titan. Alloy. 1990's (1993) 127–135.

[53] X. an Nie, Z. Hu, H. qun Liu, D. qing Yi, T. ying Chen, B. feng Wang, Q. Gao, D. chun Wang, Mater. Sci. Eng. A 613 (2014) 306–316.